AMERICAN SOCIETY FOR MICROBIOLOGY | Journal of Virology®

VIRUS-CELL INTERACTIONS

Capsid-Labelled HIV To Investigate the Role of Capsid during Nuclear Import and Integration

Irena Zurnic Bönisch,[a] Lieve Dirix,[a,b] Veerle Lemmens,[b,c] Doortje Borrenberghs,[b] Flore De Wit,[a] Frank Vernaillen,[d,e] Susana Rocha,[b] Frauke Christ,[a] Jelle Hendrix,[c] Johan Hofkens,[b] Zeger Debyser[a]

[a]Laboratory for Molecular Virology and Gene Therapy, Department of Pharmaceutical and Pharmacological Sciences, KU Leuven, Leuven, Flanders, Belgium
[b]Laboratory for Photochemistry and Spectroscopy, Molecular Imaging and Photonics, Department of Chemistry, KU Leuven, Heverlee, Flanders, Belgium
[c]Dynamic Bioimaging Lab, Advanced Optical Microscopy Centre and Biomedical Research Institute, Hasselt University, Diepenbeek, Belgium
[d]VIB Bioinformatics Core, Zwijnaarde, Belgium
[e]VIB Bioimaging Core, Leuven, Belgium

ABSTRACT The HIV-1 capsid protein performs multiple roles in virus replication both during assembly and particle release and during virus trafficking into the nucleus. In order to decipher the roles of capsid protein during early replication, a reliable method to follow its intracellular distribution is required. To complement existing approaches to track HIV-1 capsid during early infection, we developed an HIV-1 imaging strategy, relying on viruses incorporating enhanced green fluorescent protein (eGFP)-tagged capsid (CA-eGFP) protein and mCherry-tagged integrase (IN-mCherry). Wild-type infectivity and sensitivity to inhibition by PF74 point to the functionality of CA-eGFP-containing complexes. Low numbers of CA-eGFP molecules were located inside the viral core and imported into the nucleus without significant loss in intensity. Less than 5% of particles carrying both CA-eGFP and IN-mCherry retained both labelled proteins after nuclear entry, implying a major uncoating event at the nuclear envelope dissociating IN and CA. Still, 20% of all CA-eGFP-containing complexes were detected in the nucleus. Unlike for IN-mCherry complexes, addition of the integrase inhibitor raltegravir had no effect on CA-eGFP-containing complexes, suggesting that these may be not (yet) competent for integration. Our imaging strategy offers alternative visualization of viral capsid trafficking and helps clarify its potential role during integration.

IMPORTANCE HIV-1 capsid protein (CA) builds a conical shell protecting viral genomic RNA inside the virus particles. Upon entry into host cells, this shell disassembles in a process of uncoating, which is coordinated with reverse transcription of viral RNA into DNA. After uncoating, a portion of CA remains associated with the viral DNA and mediates its nuclear import and, potentially, integration into host DNA. In this study, we tagged CA with eGFP to follow its trafficking in host cells and address potential CA roles in the nucleus. We found that while functional viruses import the tagged CA into the nucleus, this capsid protein is not part of integration-competent complexes. The roles of nuclear CA thus remain to be established.

KEYWORDS CA-eGFP, HIV, capsid, fluorescence imaging, integration, nuclear import

The HIV-1 capsid protein (CA) is a 24-kDa-large structural protein which builds a conical shell inside the viral envelope (reviewed in reference 1). The capsid shell shields the viral RNA genome, the enzymes associated with it, and viral accessory proteins. The central role of the capsid protein (CA) during early HIV-1 replication steps has been well established (reviewed in reference 1). During its fusion with the host cell, HIV-1 releases a capsid core into the cytosol. The conical HIV-1 core is composed of approximately 1,500 CA monomers (2–4, 58) and has dual roles. On the one hand, it is

Citation Zurnic Bönisch I, Dirix L, Lemmens V, Borrenberghs D, De Wit F, Vernaillen F, Rocha S, Christ F, Hendrix J, Hofkens J, Debyser Z. 2020. Capsid-labelled HIV to investigate the role of capsid during nuclear import and integration. J Virol 94:e01024-19. https://doi.org/10.1128/JVI.01024-19.

Editor Frank Kirchhoff, Ulm University Medical Center

Address correspondence to Zeger Debyser, zeger.debyser@kuleuven.be.

Received 21 June 2019
Accepted 24 November 2019
Accepted manuscript posted online 15 January 2020
Published 17 March 2020

stable enough to protect viral DNA in the preintegration complexes (PICs) from degradation in the cytoplasm (5–8) and, simultaneously, it is flexible enough to allow timely uncoating coordinated with reverse transcription (9). It remains under debate how and when this uncoating occurs, either by opening of pores or a cap on the short end of the capsid core (10) or by entire core disintegration (11). Two models of the timing of uncoating prevail: cytosolic uncoating versus uncoating at the nuclear pore. Evidence for cytosolic uncoating comes from observations with HIV carrying Gag-internal green fluorescent protein (Gag-iGFP) polyprotein (12, 13); iGFP is present in viral cores and released into the cytosol within the first 30 min postfusion (11). Further support stems from findings that the sensitivity of HIV-1 to TRIM-Cyp is progressively lost during the first 4 h postinfection (14–16). In contrast to this model, other data suggest that uncoating occurs after docking to the nuclear pore. In fact, intact HIV-1 cores were observed at the nuclear envelope (NE) by electron microscopy (EM) (17), and viral DNA was found to remain protected from cytosolic degradation for a prolonged time after infection (7, 8). Recently, live-cell imaging experiments of cells transduced with CypA-dsRed-labelled HIV-1 particles demonstrated that only viruses that retain the CypA-dsRed capsid core marker until docking to the nuclear envelope are infectious (18). The latter data thus support the view that the capsid core is structurally retained until reaching the NE and only undergoes uncoating at this point.

Reverse transcription results in the formation of the viral PIC, which contains HIV DNA and integrase (IN) along with other viral and cellular proteins. Although to date no evidence exists for a direct effect of CA on integrase activity (19), recent data propose a role for CA during nuclear import of HIV-1 PICs (20–22). Whether this role is restricted to docking of PICs on the cytoplasmic side of the nucleopore (e.g., through NUP358), involves capsid uncoating when stalled in the nuclear basket (e.g., through NUP153), or is mediated by a direct interaction between capsid and nuclear import factors is not known. Despite contradictory models on the exact location of uncoating, there is a growing consensus that small amounts of CA protein can be detected in the host cell nucleus during early infection (23–25). The amount of nuclear CA is lower than what is present in intact incoming cores, and its role is not understood. Nuclear CA reportedly colocalizes with either viral DNA (vDNA) and/or the viral protein R (Vpr) (23–25, 59), but there is no consensus on whether this is a hallmark of integration-competent viral complexes. Furthermore, it remains to be shown if CA traverses the nuclear envelope in association with the PIC or by an alternative PIC-independent route. Given the interaction of CA with nucleoporins NUP153 and NUP358 (22, 26), it is possible for CA oligomers to enter the nucleus on their own and aid the active nuclear import of PIC. Furthermore, interaction between HIV-1 CA and cleavage and polyadenylation specificity factor 6 (CPSF6) has been implied to mediate CA nuclear import and targeting of CA-decorated PICs to favorable chromatin regions in the host cell nucleus (22, 27–30).

The pleiotropic role of capsid during HIV-1 replication has stimulated research on inhibitors targeting CA function/uncoating, with PF74 being one of the most investigated compounds (31, 32). PF74 binds the interhexameric interface on the capsid core lattice, perturbs capsid stability, and blocks PIC nuclear import (22, 23, 32–34, 57). At high concentrations ($\geq$10 μM), PF74 also blocks reverse transcription (23, 34, 35). PF74 can thus be used as a research tool to investigate mechanisms by which CA contributes to the formation, trafficking, and possibly integration of HIV-1 PICs.

Traditionally, CA is labelled in infected cells by immunostaining, with results and interpretations depending on the protocol used (11, 18, 23–25). For this reason, demonstrating the presence of CA in the nucleus was challenging until recently, and a consensus protocol on how to best stain for nuclear CA is lacking. Direct p24 tagging through tetracysteine motif (tC) insertions has been described before (36, 37), but this labelling still requires a secondary step of FlAsH dye attachment to the tC motif, which is technically demanding. In this study, we explored a method to enable direct imaging of the CA protein distribution in the host cells, by generating particles containing CA C-terminally tagged with enhanced green fluorescent protein (eGFP). By combining CA-eGFP labelling with mCherry-labelling of viral integrase (IN-mCherry), we can simul-

taneously track the fates of both viral proteins during early infection. We used the capsid inhibitor PF74 and the integrase strand transfer inhibitor raltegravir (RAL) to study the functionality of the CA-eGFP containing complexes in the cytoplasm and the nucleus. We believe our data provide relevant insights into the distribution of the fluorescently labelled HIV-1 CA, making it a useful tool to study early HIV-1 replication steps.

RESULTS

A new and direct HIV-1 capsid labelling strategy. To attempt and simplify CA tagging inside infected cells, we developed a direct capsid labelling strategy through fusion of CA with eGFP. We started by comparing insertions or terminal attachments of tC tags with terminal attachments of eGFP to CA (Fig. 1A and C). We used two different tC tags: the short CCPGCC (for insertions within the CA sequence) (Fig. 1A and B) and the longer modified tag FLNCCPGCCMEP (38) (for N- and C-terminal tagging of the CA) (Fig. 1C), which has an increased affinity for FlAsH and increases signal quantum yield. As outlined in Materials and Methods, we used two different linkers for the tagging of CA with eGFP, based on the described linker properties (39) and to facilitate minimal interference with CA structure (Fig. 1C). To attach eGFP to the N terminus of CA, we used a flexible glycine-serine linker (GGSGT), and for the C-terminal fusion, we used a proline-kink (DPPVAT) linker. We next assessed the tC and eGFP N- and C-terminal fusions to CA for their ability to support efficient virus production (Fig. 1D). We produced replication-deficient viruses containing only the tagged CA versions and those with different ratios of tagged to untagged CA. The ratios refer to the amounts of coding plasmids used for transfection. Virus particles were concentrated, and particle release was measured by p24 enzyme-linked immunosorbent assay (ELISA) and SYBR green product-enhanced reverse transcriptase (SG-PERT; see Materials and Methods). All labelling approaches resulted in reduced particle release and infectivity (Fig. 1D), in line with the described fragility of the CA for proper cone formation (2). Additionally, we measured the single-round transduction efficiency of all tagged viruses, using a luciferase reporter in HeLa P4 cells (Fig. 2). Lowering the ratio of CA-eGFP to untagged CA in the particles to 1:10 rescued the transduction capacity of all dually tagged particles. In contrast, the 1:2 ratio of CA-eGFP versus untagged CA only yielded luciferase signals with eGFP-tagged CA and the N-terminally positioned tC tag in CA (N-terminal tC and tC_{4-9}). Viruses produced with only the tagged CA versions (ratio 1:0 in the figure legend) were unable to transduce target cells (Fig. 2). In further experiments, we tested if these labelled particles can be visualized by fluorescence microscopy through either FlAsH labelling (for tC-modified CA; data not shown) or by eGFP fluorescence (data not shown). Since it was not possible to perform successful FlAsH labelling despite extensive optimization according to published protocols (11, 36), we decided to continue with the CA construct C-terminally tagged with eGFP (CA-eGFP).

To develop an integrated particle visualization approach, the CA labelling strategy was applied to a previously established and characterized virus-labelling system containing the fluorescently tagged IN (40, 41). Briefly, in this system, the IN protein with a C-terminal fluorescent tag (IN-FP) is packaged into virions by Vpr-mediated transincorporation. After proteolytic cleavage from Vpr, the IN-FP fusion becomes a functional component of the viral PIC. As a modification of this approach and to make IN labelling compatible with CA-eGFP, we used the mCherry-tagged IN in the same vector (IN-mCherry). We first validated the use of IN-mCherry in our system, by comparing particle release and transduction efficiency of IN-mCherry-containing particles with the previously published IN-eGFP-labelled viruses (Fig. 3) (41, 42). Both the p24 ELISA and quantitative reverse transcriptase (RT) tests showed comparable virus production efficiencies (Fig. 3A). Subsequently, normalized amounts of each virus (according to either p24 ELISA or SG-PERT quantitative PCR [qPCR]) were used to transduce HeLa P4 cells, and single-round infectivity was assayed by luciferase reporter (fLuc) readout 3 days

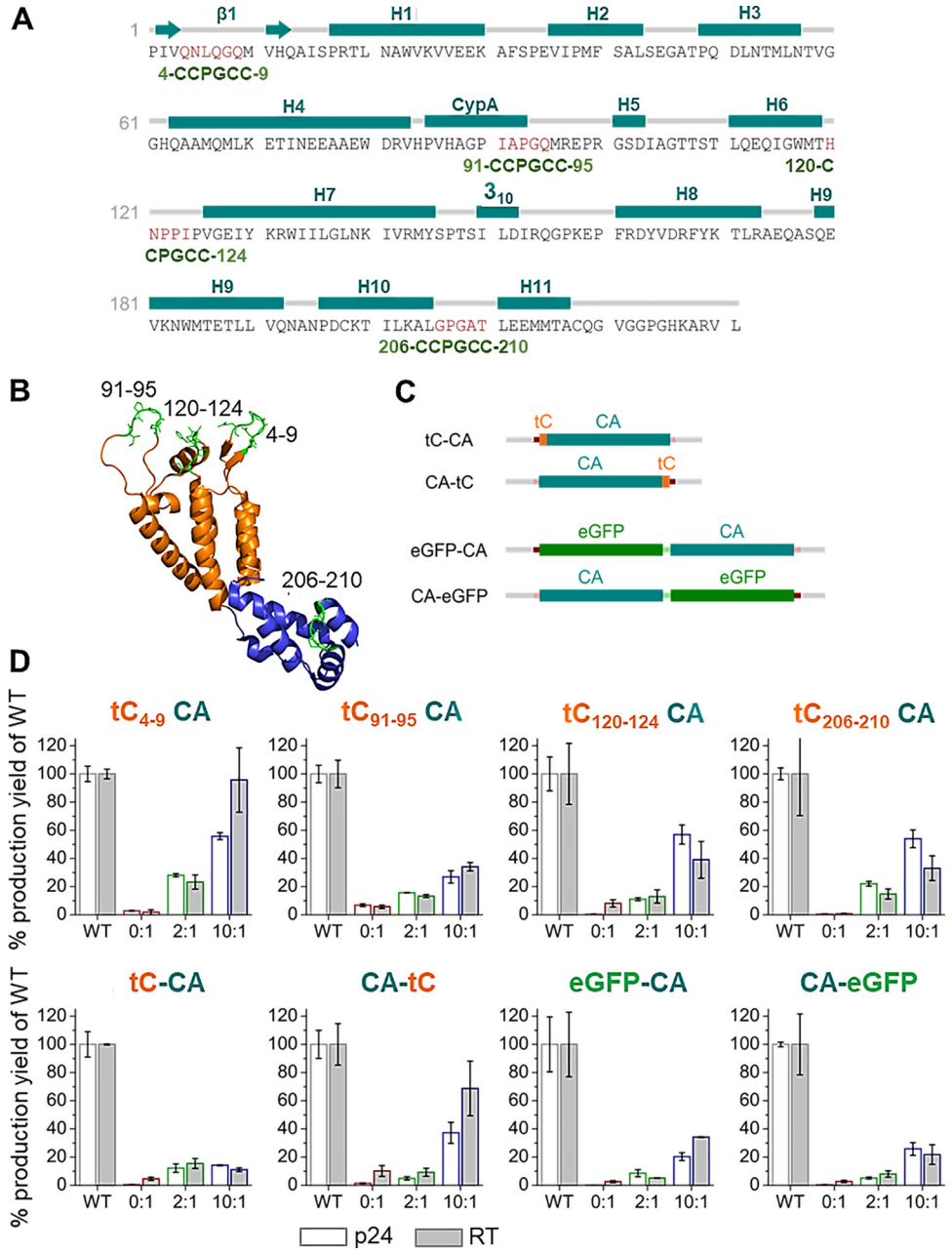

FIG 1 Schematic representation of CA tagging strategies. (A) Amino acid sequence and primary structure of HIV-1 CA, with tC motif insertions highlighted in light green below the sequence. Important alpha helices and domains are marked in dark green on the level of the sequence. H1 to H11, alpha helices number 1 to 11; CypA, cyclophylin A binding motif; B1, beta sheet 1. (B) Secondary structure of a CA monomer, as found in the CA hexamer (PDB 3H4E), with tC insertions highlighted in light green, corresponding to that in panel A. Orange, N-terminal domain (NTD); blue, C-terminal domain (CTD). (C) Schematic representation of tC or eGFP tag fusions to the CA N or C terminus, respectively. Reintroduced protease cleavage sites are indicated in dark red and linkers for optimal eGFP folding are indicated in light green. tC tags are highlighted in orange. (D) Recombinant, VSV-G pseudotyped virus particles were produced by transfection as outlined in Materials and Methods. For transfections, different ratios of the pNL4-3.Luc.R-E- derivatives (coding for either the tC- or the eGFP-tagged CA) and the original pNL4-3.Luc.R-E construct were mixed as indicated on the *x* axes (0:1, 1:0, 1:2, and 1:10). The positions of tC and eGFP tags in each virus prep are indicated above corresponding plots. Virus particles were harvested and filtered, and particle release was assessed by p24 ELISA and SG-PERT (indicated RT). Particle release values of viruses carrying only the original pNL4-3.Luc.R-E- construct (WT) were arbitrarily set to 100%, and error bars represent standard deviations from triplicates. Data are derived from one representative of $n = 2$ independent experiments.

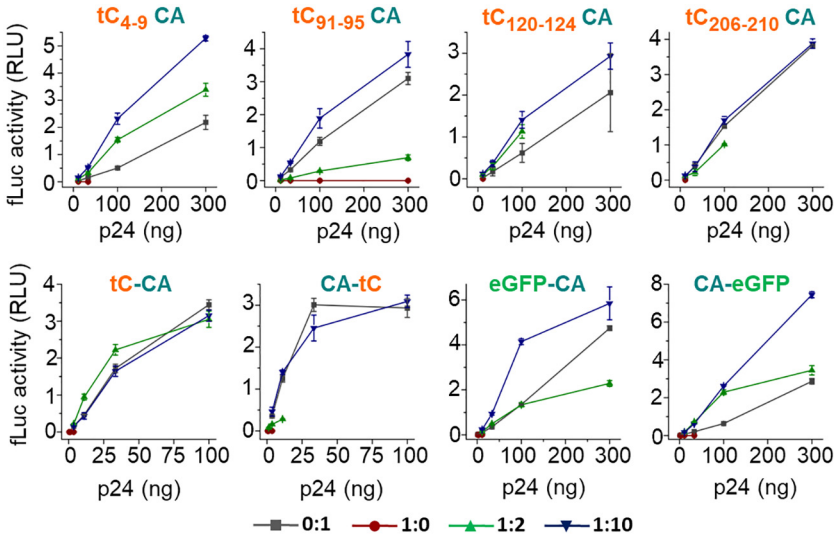

FIG 2 Transduction efficiency of single- and dually labelled viruses (accompanying Fig. 1). Recombinant, VSV-G pseudotyped virus particles were produced by transfection as outlined in Materials and Methods. For transfections, different ratios of the pNL4-3.Luc.R-E- derivatives (coding for either the tC- or the eGFP-tagged CA) and the original pNL4-3.Luc.R-E construct were mixed as indicated at the bottom. The positions of tC and eGFP tags in each virus prep are indicated above the corresponding plots. Virus particles were harvested and filtered, and particle release was assessed by p24 ELISA. Transduction efficiencies of these particles were evaluated 3 days posttransduction of HeLa P4 cells and are represented as RLU values of the fLuc reporter readout. Error bars represent standard deviations from triplicates. Data are derived from one representative of $n = 2$ independent experiments.

posttransduction (Fig. 3B and C). Both the IN-mCherry- and IN-eGFP-labelled viruses efficiently transduced target cells, demonstrating the functionality of these viruses. To ensure that the IN-FP incorporation and labelling efficiency were comparable between these two virus species, we spotted purified and concentrated viruses on coverslips and immunostained them with the p24 antibody (Fig. 3D). We observed that the fluorescence background was higher in the IN-mCherry channel (Fig. 3D, top) which impaired reliable determination of particle labelling efficiency, in contrast to that for IN-eGFP-containing viruses (Fig. 3D, bottom). Since the high mCherry background could also originate from background fluorescence of extracellular vesicles or the coverslip surface, we decided to validate these viruses in virus-imaging experiments. Transduced HeLa P4 cells were fixed 6 h postinfection, and IN-FP localization and content were probed by the IN-FP intracellular distribution (Fig. 3E), efficiency of nuclear entry (Fig. 3F), and IN-FP fluorescence intensity profiles (Fig. 3G) as described previously (41). Since all data were comparable between the two viral species, without background interference in the IN-mCherry channel, we conclude that IN-mCherry is a suitable particle label. Hence, we continued with further characterization of double-labelled viruses containing IN-mCherry and CA-eGFP.

To produce capsid-labelled virus particles, we used a mixture of pNL4.3.Luc.R-E-based plasmids coding for tagged and untagged CA at different ratios: 1:0, 1:2, 1:10, or 0:1, respectively (CA-eGFP coding vector versus untagged, original pNL4.3.Luc.R-E-vector). This pNL4.3.Luc.R-E- mixture was transiently cotransfected with Vpr-IN-mCherry- and vesicular stomatitis virus (VSV)-G-encoding constructs into 293T cells to produce double-labelled HIV-1 particles (Fig. 4A). As a reference, unlabelled particles (termed WT) and single- labelled particles (termed wild-type-mCherry [WT-mCh]) were produced by transfection of the original pNL4.3.Luc.R-E- in combination with only the VSV-G-encoding or both the VSV-G- and IN-mCherry-encoding constructs, respectively. Vpr transincorporation of fluorescently tagged Vpr-IN is known not to influence single-round virus infectivity (40, 41), as confirmed in this study (compare WT and WT-mCh conditions in Fig. 4C). Virus production efficiency was determined by the endogenous RT-qPCR test. We confirmed that fusing an eGFP tag to p24 CA diminishes virus particle

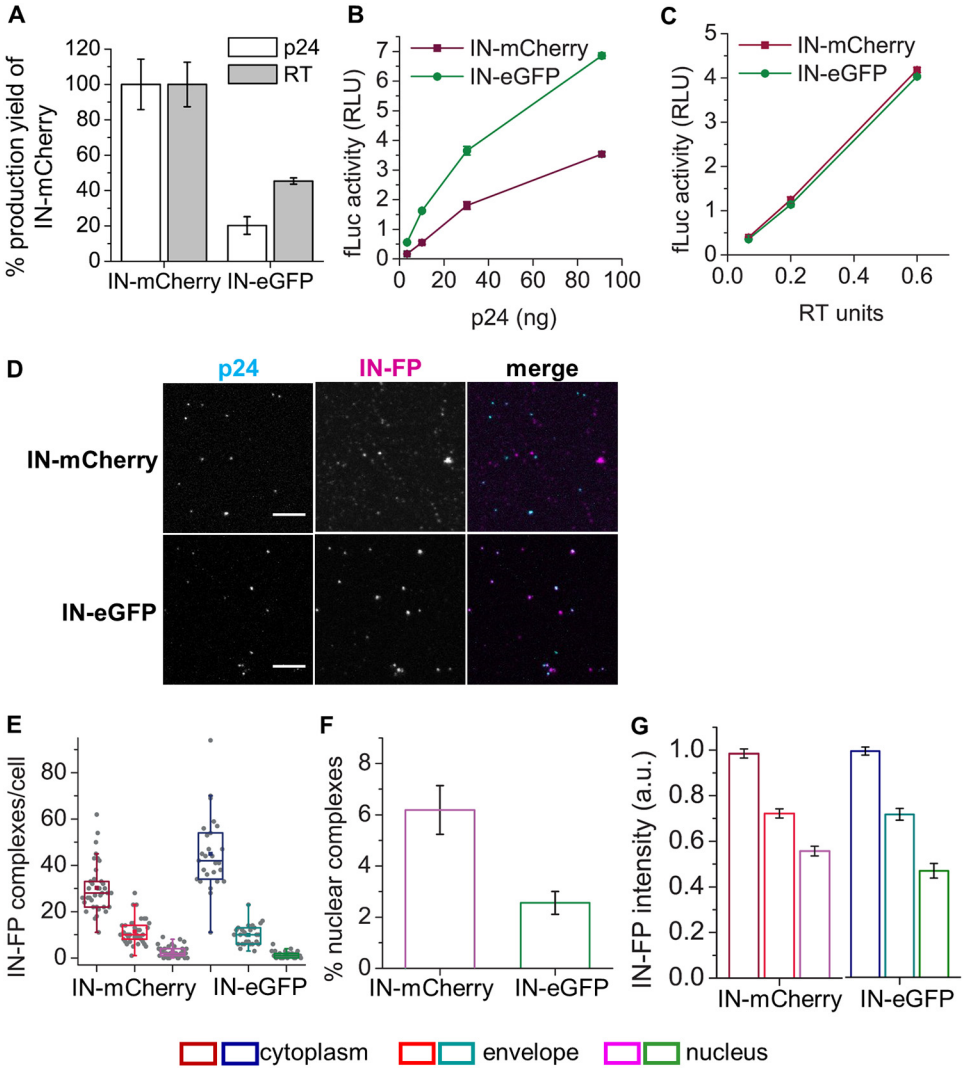

FIG 3 IN-mCherry labelling yields particles comparable with IN-eGFP-containing virions. Replication-deficient virus particles were produced by transiently transfecting 293T cells with pNL4-3.Luc.R-E-, pVpr-IN-FP (IN-mCherry or IN-eGFP, indicated on the *x* axes), and pVSV-G constructs. (A) Virus particle release was quantified by p24 ELISA and SG-PERT (RT activity) of purified particles and expressed relative to one another. The yields of IN-mCherry containing viruses were arbitrarily set to 100%. The data represent means ± standard deviations (SDs) from triplicates. (B) HeLa P4 cells were transduced with normalized amounts of fluorescent viruses, and firefly luciferase (fLuc) reporter levels were assayed 3 days posttransduction. Luciferase readout was normalized to the total protein input (determined by BCA assay) and expressed as relative light units (RLU). Data are means ± SDs from triplicates. (C) RLU values according to RT units. (D) Representative images of purified viruses containing IN labels (IN-eGFP and IN-mCherry). Particles were adhered to microscopic slides for 4 h at 37°C and were then fixed with PFA and immunostained using AG3.0 p24 antibody. The channels in which p24 staining (blue) or IN-FP fluorescence (magenta) were detected are indicated in corresponding pseudocolors. For each type of particles, the merged image is shown at the end of each panel as the overlay of two pseudocolors. The overall image brightness was improved in ImageJ software for clarity purposes. Scale bars, 5 μm. (E to G) HeLa P4 cells were transduced with IN-FP labelled viruses and fixed 6 h postinfection; nuclear envelope was defined by lamin A/C immunostaining. The cells were imaged by confocal microscopy, and numbers and fluorescence intensities of IN-FP complexes were determined in each subcellular compartment (cytoplasm, nuclear envelope, nucleus; consult Fig. 7A for clarification). Data are derived from $n = 1$ experiment. (E) The number of IN-FP complexes per cell is represented by box-and-whisker plots for each virus. (F) Percentage of nuclear IN-FP complexes per condition. The percentage was calculated as the fraction of IN-FP complexes localized in infected cell nuclei compared to the total number of IN-FP complexes detected in the experiment. Error bars represent SD values. (G) IN-FP complex intensities were measured as previously described (41) and plotted for each compartment (cytoplasm, nuclear envelope, and nucleus). The bars represent the mean ± SD values. As indicated elsewhere, the intensities significantly differ between the cytoplasm and the nucleus ($P < 0.001$, two-tailed *t* test with equal variance assumed).

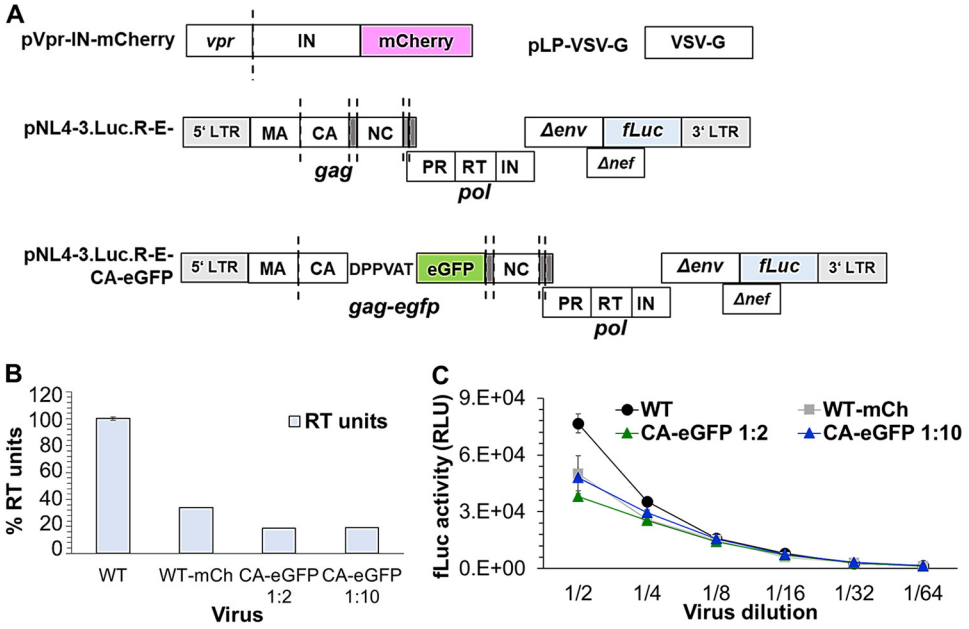

FIG 4 Schematic outline of the experimental setup and optimization of fluorescent CA labelling. (A) Constructs used for fluorescent labelling of replication-deficient, VSV-G pseudotyped virus particles. The eGFP tag was fused to the C terminus of capsid via the DPPVAT linker, in the context of the pNL4-3.Luc.R-E- transfer and packaging construct. mCherry was fused to the integrase C terminus by replacement of the eGFP open reading frame (ORF) with the mCherry ORF in the context of the pVpr-IN-FP construct (40–42). Labelled virus particles were produced by transient transfection of pLP-VSV-G, pVpr-IN-mCherry, pNL4-3.Luc. R-E-, and (only for double-labelled viruses) pNL4-3.Luc.R-E- CA-eGFP into 293T cells. Virus supernatants were harvested and concentrated as described in Materials and Methods. Dashed lines indicate viral protease cleavage sites. Δ*env* and Δ*nef* indicate *env* and *nef* shortened open reading frames, respectively. (B) Unlabelled particles (WT), particles with IN-mCh (WT-mCh), and double-labelled particles (CA-eGFP) containing also the labelled capsid (using pNL4-3.Luc.R-E- CA-eGFP and WT pNL4-3.Luc.R-E- constructs at a ratio of 1:2 or 1:10) were produced as described above. Endogenous reverse transcriptase activity was assessed by SG-PERT. Values are derived from one experiment. Data are presented normalized to the unlabelled (WT) virus levels. (C) Single-round transduction efficiencies of unlabelled and labelled virions. Unlabelled, single-, and double-labelled viruses were produced and concentrated as described in Materials and Methods. Unlabelled particles (WT) were produced by transfection of the parental luciferase-coding vector in combination with the VSV-G-coding plasmid. Single-labelled particles contained IN-mCherry after addition of Vpr-IN-mCh to the parental luciferase construct. Double-labelled particles all contained IN-mCherry and CA-eGFP produced with a CA-eGFP to WT pNL4-3.Luc.R-E- vector ratio of 1:2 or 1:10, respectively. Single-round transduction efficiency was determined by firefly luciferase (fLuc) levels in HeLa P4 cells transduced with serial dilutions of virus supernatants (starting amounts were normalized for endogenous RT activity, and virus dilutions are shown on the *x* axis). Relative light units (RLU) were measured 3 days posttransduction and represent a relative value obtained after normalizing the fLuc signal for protein content using the BCA assay. Data are derived from one experiment.

release, which can be restored to various levels by producing particles with a mixture of untagged and tagged CA (Fig. 1D and 4B). Estimating the functionality of these particles for single-round transduction, we observed that increasing the ratio of untagged to eGFP-tagged CA in the virions rescued single-round transduction efficiency (Fig. 4C). Hence, it is possible to introduce the eGFP label to the HIV-1 capsid without detrimental effects on particle release and virus transduction efficiency.

Next, we addressed the CA-eGFP labelling efficiency and the extent of dual particle labelling (Fig. 5). To this end, we spotted the single- or double-labelled particles in 8-well microscopy chambers and fixed and stained them with the capsid-specific monoclonal antibody to determine the percentage of particles (all foci stained with p24 antibody) containing CA-eGFP (Fig. 5A). Based on previous data reporting high particle labelling efficiency for IN-eGFP (42), we expected IN-mCherry to be present in a comparable fraction of all particles. As previously shown (Fig. 3D), the relatively high fluorescence background in the mCherry channel hampered an exact estimation of IN-mCherry labelling efficiency in the virus particles. When looking at the CA-eGFP positive foci, about 30% of particles (as detected by p24 immunostaining) contained the capsid label (Fig. 5B).

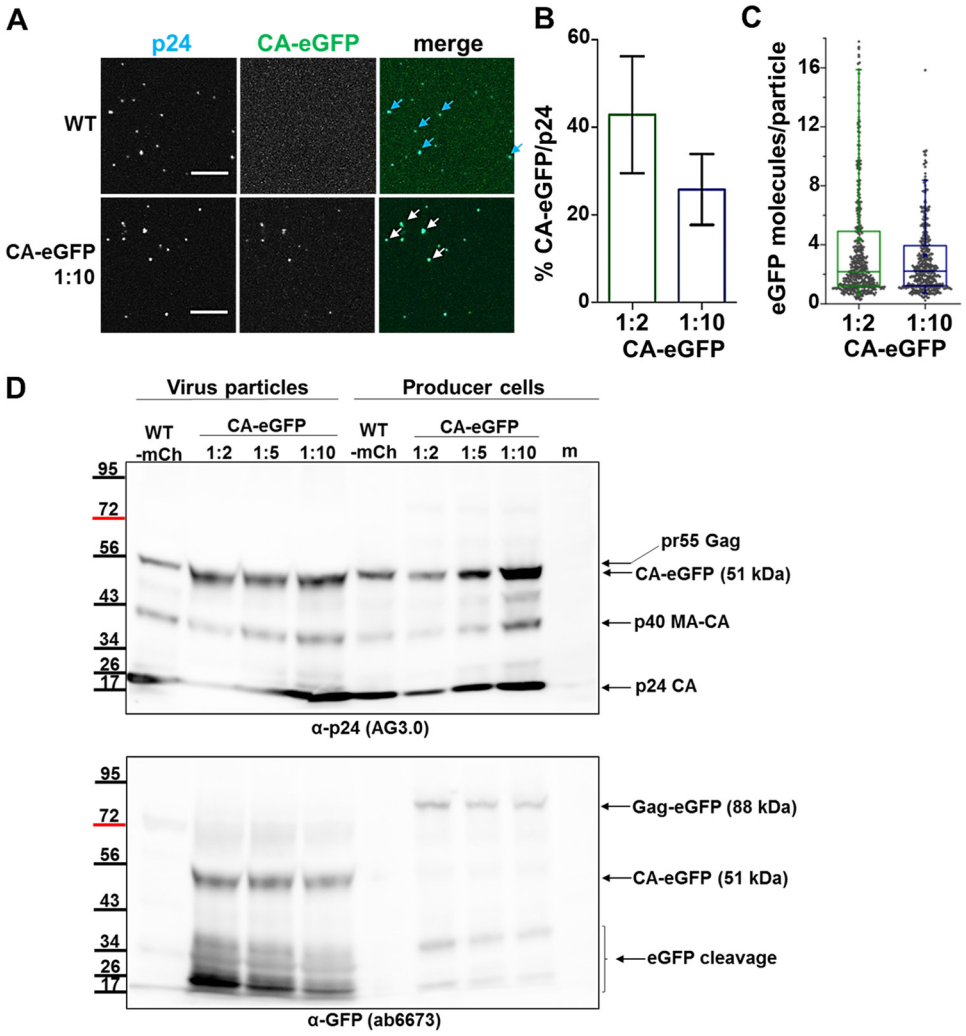

FIG 5 CA-eGFP is incorporated into extracellular HIV-1 virions. Virions containing only the IN-mCherry label are marked as WT-mCh, while double-labelled virions (containing CA-eGFP in addition to IN-mCherry) are always indicated as CA-eGFP, with the ratio of labelled to unlabelled capsid (pNL4-3.Luc.R-E- CA-eGFP to WT pNL4-3.Luc.R-E-) 1:10 in the annotation. Data are derived from one representative of $n \geq 3$ experiments. (A) Virus particles were allowed to attach to microscopic slides for 4 h at 37°C and were then fixed and immunostained with AG3.0 p24-specific antibody followed by secondary antibody conjugated to Alexa 405. Fluorescent signals originating from p24 staining (blue), IN-mCherry (not shown; see Fig. 3D) and CA-eGFP (green) are shown in corresponding pseudocolors. Overlay of the channels showing p24 staining and CA-eGFP signals is shown under "merge" panels. (Top) Particles containing only IN-mCherry (single-labelled viruses); (bottom) particles containing both IN-mCherry and CA-eGFP labels, where ratio of labelled to unlabelled pNL4-3.Luc.R-E- vector was 1:10. Particles only stained by p24 are indicated by blue arrows, while those in which the CA-eGFP label colocalizes with p24 staining are indicated by white arrows. The overall image brightness was improved in ImageJ software for clarity purposes. Scale bars, 5 μm. (B) CA-eGFP labelling efficiency was determined as the percentage of all p24-stained particles that also contained CA-eGFP. The labelling efficiency is shown for both CA-eGFP 1:2 and CA-eGFP 1:10 particles, where the values are plotted as the means ± standard deviations. Data are derived from $n \geq 3$ independent experiments. (C) The number of CA-eGFP molecules per particle was determined in comparison with a monomeric eGFP solution, both of which were imaged by wide-field TIRF microscopy as in Materials and Methods. The ratio of the fluorescence intensity of the spotted particles to that of monomeric eGFP was used to estimate CA-eGFP incorporation into single virions. (D) Recombinant virus particles and 293T producer cells were lysed with 1% SDS, and proteins were separated on a gradient gel (4% to 15%) SDS-PAGE. HIV capsid (CA; p24) and eGFP were detected with the corresponding antibodies, annotated below each figure panel. A molecular weight ladder is present next to each membrane, and expected protein sizes are indicated by arrows. As in panel A, single- and dual-particle labelling is indicated at the top of each panel (WT-mCh or CA-eGFP). For producer cell lysates, the marking indicates constructs used for transfection (in addition to the pLP-VSV-G and NL4-3-based transfer vector): WT-mCh indicates only Vpr-IN-mCherry was transfected, while CA-eGFP 1:2, 1:5, and 1:10 indicate additional cotransfections of the CA-eGFP coding transfer vector at the respective ratios. One representative experiment is shown for $n = 2$ experiments.

Based on the one-to-ten CA-eGFP-to-parental pNL4-3.luc construct ratio during virus production, we expected that one-tenth of all CA molecules in the virion would be labelled with eGFP. This theoretically amounts to about 400 CA-eGFP molecules out of a total of 4,000 CA monomers (4). Thus, we next determined how many CA-eGFP monomers were part of the mature virions. To this end, we subjected purified and concentrated CA-eGFP-labelled virions to single-particle intensity analysis using wide-field total internal reflection fluorescence (TIRF) microscopy (Fig. 5C), as described previously (42). In brief, we coated coverslips with CA-eGFP virus solutions at concentrations at which single viruses could be discriminated and compared the intensity determined by two-dimensional (2D) Gaussian fitting of these viruses with the intensity of coated single eGFP molecules. From the single virus intensity, we determined that between one and four eGFP molecules (indicative of the same number of CA-eGFP monomers with a median number of two) are found in the labelled viruses. Thus, the CA-eGFP labelling efficiency of the recombinant HIV-1 virions is low, which may result from the sterical hindrance the eGFP tag exerts on the capsid core.

To confirm that the eGFP signal in imaged viruses originated from the CA-eGFP fusion and not free eGFP, we lysed concentrated virus particles and virus-producing 293T cells and subjected these lysates to Western blotting (Fig. 5D). We produced viruses containing either only IN-mCherry (WT-mCh lanes) or both IN-mCherry and CA-eGFP (CA-eGFP lanes). In these experiments, we produced CA-eGFP-tagged viruses by cotransfecting three different ratios of the CA-eGFP luciferase transfer vector to the parental vector (1:2, 1:5, and 1:10, as indicated above the blot). We detected Gag and capsid protein variants in these samples using both the p24- and GFP-specific antibodies. Nontransfected cell lysates (labelled mock [m]) were used as a negative control. We detected both the Gag precursor protein with additional eGFP (pr55 Gag-eGFP) and CA-eGFP in virus-producing cells transfected with the pNL4-3.Luc.R-E-based vector mixtures. When analyzing virus particle lysates, we observed a dominant CA-eGFP band as well as minor bands corresponding to the Gag precursor (Gag-eGFP) or intermediate cleavage products (60–62) (Fig. 5D). CA-eGFP is apparently correctly processed from the precursor protein and is encapsidated in the virions, and our sensitive imaging system allows us to detect low numbers of intraparticle CA-eGFP monomers.

To exclude the possibility that CA-eGFP is located outside the viral cone, we next determined the intraparticle location of CA-eGFP monomers by permeabilizing the particles with saponin (43) (Fig. 6A). We mounted the purified double-labelled viruses onto slides and subjected them to a 5-min treatment with either phosphate-buffered saline (PBS) or saponin. Saponin punctures small holes in the viral membrane, causing all proteins not stably associated with the core or embedded in it to dissociate. In the absence of saponin, viral particles are intact, and so both IN-mCherry and CA-eGFP should be detected as clear fluorescent foci. Important to note is that such short saponin permeabilization will not cause dissociation of HIV-1 cores, unlike treatments described elsewhere (44). As shown in Fig. 6B, after PBS treatment of virus particles, eGFP foci (indicative of CA-eGFP) remained intact and associated with p24 (Fig. 6B, PBS panel). If CA-eGFP is monomeric and free outside the viral core, saponin treatment should release it into the medium and the eGFP foci should disappear. Despite the loss of approximately 50% of the particles under saponin treatment (fewer detected p24 foci, possibly due to inadvertent lysis or release of p24 and CA-eGFP molecules from defective particles), eGFP foci were retained in the presence of saponin and largely colocalized with the p24 foci (Fig. 6B, saponin panels). To determine the amount of CA-eGFP associated with the cores before and after saponin treatment, we quantified eGFP fluorescence (Fig. 6C). We observe a mere 1.5-fold loss of CA-eGFP signals in saponin-permeabilized particles. These data indicate that the majority of CA-eGFP is either incorporated into or encased by the capsid core. These findings were corroborated by capsid core purification experiments, where intact cores of CA-eGFP-labelled HIV particles were purified through a sucrose gradient (as described previously in reference 45) (Fig. 6D). The core fractions were pooled, adhered to microscopic slides, and stained with p24 antibody (Fig. 6E). Colocalization between CA-eGFP and immu-

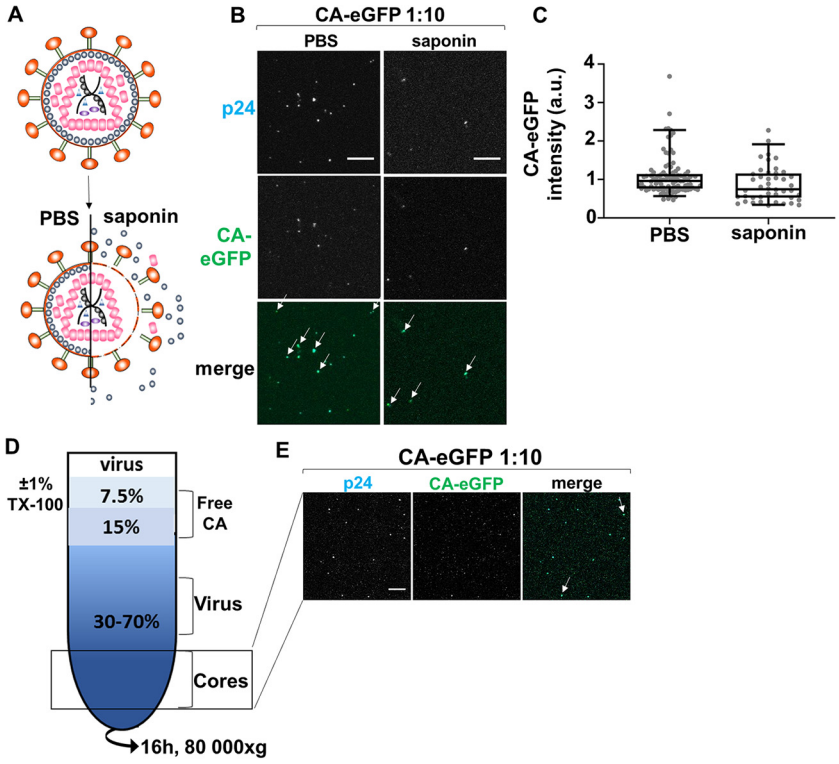

FIG 6 eGFP-tagged capsid is associated with the viral core. (A) Schematic outline of saponin-mediated particle permeabilization (adapted from reference 43). Saponin punctures small pores in the viral membrane, causing all content not stably incorporated in the capsid core or embedded inside the core to dissociate. Upon washing, only the core-associated content remains. (B) Recombinant virus particles were produced to contain IN-mCherry and CA-eGFP and mounted on poly-D-lysine-coated microscopic slides (see Materials and Methods). The particles were treated for 5 min with either PBS or 100 μg/ml saponin, washed, fixed in 4% PFA, and immunostained with p24 specific antibody (AG3.0). IN-mCherry (not shown), CA-eGFP, or p24-Alexa 405 fluorescence was detected in corresponding fluorescence channels, and particles were identified by in-house Matlab routines. Merged images were produced to show overlap of all three channels. White arrows indicate overlap of the three fluorophores, indicating intact capsid cores. Scale bars, 5 μm. (C) Fluorescence intensities of CA-eGFP in PBS or saponin-treated virus particles. Viruses were analyzed by an in-house Matlab routine, as described in Materials and Methods. Intensities are plotted in 5% to 95% box-and-whisker plots. Data are derived from one representative of $n = 3$ independent experiments. (D) Schematic outline of HIV-1 capsid core purification (as described in reference 45). Recombinant virus particles were produced as described (see Materials and Methods) and pelleted by ultracentrifugation through a 20% sucrose cushion. The particles were resuspended in cold STE buffer and loaded atop several layers with increasing concentrations of sucrose dissolved in STE buffer. In the presence of Triton in the 15% sucrose layer, the virus membrane is stripped off the particles during centrifugation. The cores remain intact and accumulate in the lowest fractions during centrifugation. In the absence of Triton, virus particles remain intact and accumulate in the middle gradient fractions due to their lower density than the viral cores (1.18 g/ml density in comparison to 1.24 g/ml density of cores). (E) Viral cores were purified by ultracentrifugation of concentrated particles through the detergent layer and continuous sucrose cushion, and fractions containing viral cores were collected and combined. The core suspension was attached to microscopic slides for 20 min at room temperature, after which the samples were fixed and immunostained with the p24-specific antibody (mouse AG3.0). The cores were imaged under the confocal microscope and identified by in-house Matlab routines. White arrowheads denote complexes containing CA-eGFP, which also stained positive for p24. The overall image brightness was improved in ImageJ software for clarity purposes. Scale bar, 5 μm.

nostained CA in the core fractions suggests that fluorescently labelled capsid molecules are part of the capsid cone or reside inside. We also visualized the IN-mCherry fluorescence under conditions with and without saponin (data not shown), and we observed identical profiles under both conditions, although with significant fluorescence noise as mentioned above. After this initial validation, we set out to explore our combined labelling approach for single-virus imaging.

Labelled integrase and capsid proteins display distinct intracellular distributions during early HIV transduction steps. After successful incorporation of CA-eGFP

into HIV-1 particles, we next investigated whether CA-eGFP could be detected in transduced host cells and how its distribution correlated with that of IN-mCherry complexes. We used HeLa P4 cells for single-virus imaging, because the cytoplasm-to-nucleus volume ratio is large enough to reliably localize fluorescent virus complexes to either the cytosol, the nuclear envelope (NE), or nucleus and to study the requirements of HIV-1 nuclear import (reviewed in references 1 and 46). HeLa P4 cells were transduced with single- or double-labelled virions for 6 h and then fixed and stained to identify the nuclear lamina (Fig. 7A). Using in-house Matlab routines, we determined the numbers and fluorescence intensities of IN-mCherry and/or CA-eGFP complexes in the cytoplasm, at the NE, and in the nucleus as three main compartments (Fig. 7 and Table 1).

As shown in Fig. 7, nuclear import of all labelled viral complexes was detected at 6 h posttransduction (Fig. 7B and D). Consistent with previous data (41), at this moment, approximately 15% and 5% of all IN-mCherry-containing PICs were detected at the NE and in the nucleus, respectively (Fig. 7B and Table 1). The IN-mCherry distributions were comparable between single- and double-labelled virions, indicating that CA-eGFP labelling does not interfere with the nuclear import of PICs labelled with fluorescent IN. The data were largely comparable among the viruses, except that particles with a higher CA-eGFP content (CA-eGFP 1:2) were impaired by 50% for nuclear import (Fig. 7B and Table 1). This correlates well with the lower transduction efficiency of these recombinant virions (Fig. 4C). See Table 2 for an overview of numbers of nuclear complexes containing either one (IN-mCherry only, CA-eGFP only) or both (IN-mCherry+CA-eGFP) fluorescent labels.

While most IN-mCherry complexes were in the cytosol at 6 h, the intracellular distribution of the CA-eGFP-containing complexes was markedly different (compare Fig. 7B and D). Unlike the labelled IN, 80% of all CA-eGFP complexes distributed equally between the cytosol and the nuclear envelope, and the remaining 20% were detected in the nucleus (Fig. 7D).

In addition to the localization profiles, we also determined fluorescence intensities of the viral complexes (Fig. 7C and E). Nuclear IN-mCherry complexes had a significantly lower intensity than their cytosolic counterparts, confirming previous findings (41) on reduced IN content of nuclear PICs (Fig. 7C). In striking contrast, no significant change in CA-eGFP fluorescence intensities between the different compartments was seen (Fig. 7E). Note that any loss of CA-eGFP from the core and/or the viral PIC would result in "invisible" capsid complexes, due to the low level of CA-eGFP molecules (median $n = 2$) per particle. Our data imply that either intact capsid cores gain access into the nucleus if CA-eGFP is a measure of overall CA or that the few CA-eGFP monomers present inside the viral core are imported into the nucleus. While discrete changes in CA-eGFP intensity could not be reliably observed, we also analyzed the fraction of high-intensity ($>$1.5 arbitrary units [AU]) CA-eGFP-labelled particles in the three main intracellular compartments (cytosol, nuclear envelope, and nucleus) (Fig. 7F). This type of analysis included the complexes equivalent to the top 15% highest-intensity cytosolic CA-eGFP complexes. We observed a higher fraction of these bright CA-eGFP foci in the cytosol than in the NE and the nucleus, indicating that part of CA-eGFP is lost from PICs while trafficking from the cellular to nuclear membrane or that PICs with a higher CA-eGFP content, perhaps also in the cone, do not make it into the nucleus.

The difference in relative fluorescent PIC distribution may point to differences in the dynamics of nuclear import between the labelled capsid and integrase complexes. This notion is also supported by the data obtained on complexes containing both IN-mCherry and CA-eGFP (Fig. 7G). At 6 h postinfection, between 18% and 23% of all cytosolic IN-mCherry complexes contained CA-eGFP, whereas this colocalization rate dropped to 15% at the nuclear envelope and to 7% in the nucleus. The largest difference between IN-mCherry and CA-eGFP distribution was observed at the NE (compare Fig. 7H and I). The percentage of IN-mCherry complexes containing CA-eGFP dropped only slightly between cytosol and the NE (Fig. 7H) in contrast to CA-eGFP complexes, where the fraction colocalizing with IN-mCherry was 4-fold reduced at the

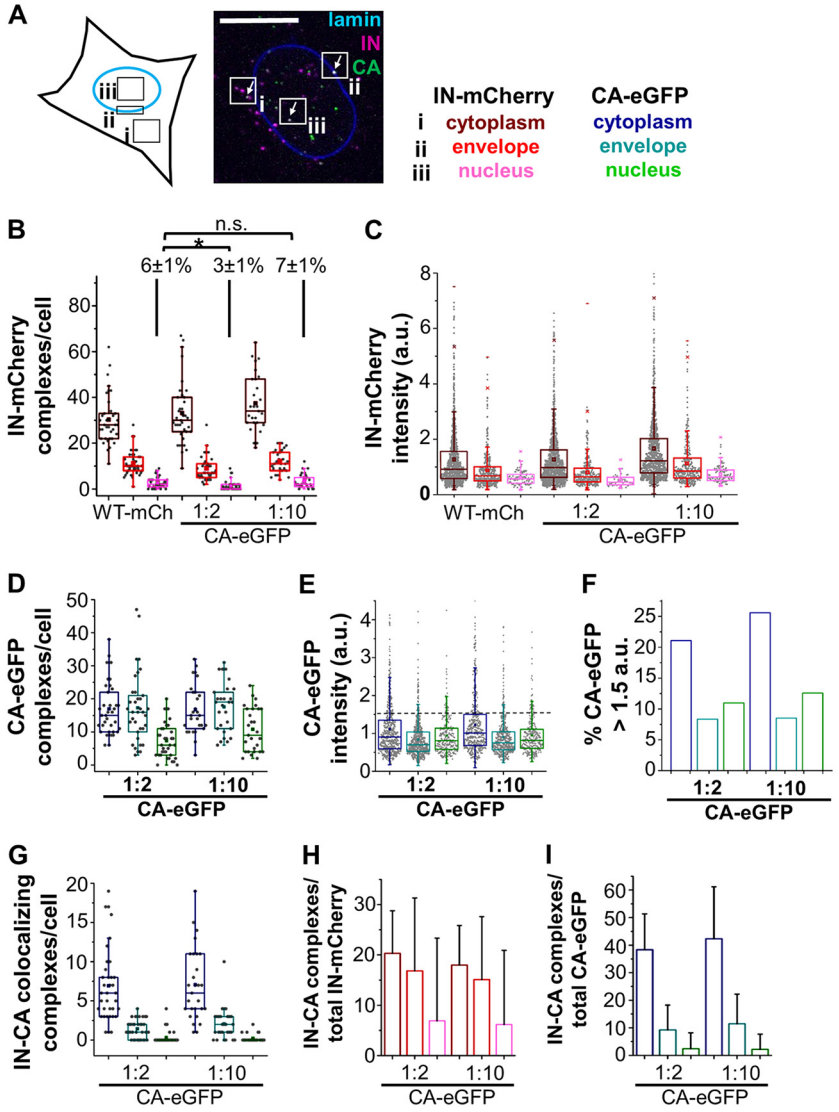

FIG 7 IN-mCherry and CA-eGFP complexes display distinct subcellular distributions early on after infection. Recombinant and fluorescently labelled viruses were produced as outlined in the legend for Fig. 4A. WT-mCh particles contain only the IN-mCherry protein, and their cell entry features were compared to those of double-labelled viruses containing CA-eGFP at different ratios to unlabelled capsid (1:2 and 1:10, as annotated on the graphs). (A) Workflow of a single-virus imaging experiment. HeLa P4 cells were transduced with single- or double-labelled viruses, fixed and immunostained with a nuclear lamina-specific antibody. The stained nuclear lamina is used as a reference to localize fluorescent viral complexes to either the cytoplasm (i), the nuclear envelope (ii), or the nucleus (iii). Cells were imaged by laser scanning confocal microscopy in z-stacks. The image on the right shows a representative z-stack of a HeLa P4 cell transduced with IN-mCherry and CA-eGFP-labelled virions 6 h posttransduction. The nuclear envelope is indicated by lamin staining (blue), and IN-mCherry- and CA-eGFP-containing viral complexes are depicted in magenta and green, respectively. White arrows indicate double-labelled fluorescent viral complexes. Scale bar, 10 μM. For each experiment, cells were imaged in z-stacks, with a 0.3-μm step size, and viral complexes were identified by an in-house Matlab routine as described previously (41). Each fluorescent viral complex was automatically detected and localized using in-house Matlab routines. (B to I) HeLa P4 cells were transduced with recombinant particles, and fluorescent complexes were identified and characterized in these cells 6 h after transduction using in-house Matlab routines. Based on nuclear lamina staining, viral PICs were assigned to one of the three intracellular compartments (cytoplasm, nuclear envelope, and nucleus). Numbers (B, D, and G) and fluorescence intensities (C and E) of viral complexes were measured for each complex and are shown for IN-mCherry (B and C) and CA-eGFP (D and E). Shown are the data from one representative of $n = 2$ experiments. The complex numbers and intensities are plotted into 5% to 95% box-and-whisker plots, where the line in the box represents the median number and whiskers represent outliers. (B) Intracellular distributions of IN-mCherry labelled complexes after transduction of HeLa P4 cells with single- (WT-mCh) or double-labelled (CA-eGFP 1:2 and CA-eGFP 1:10) virions. Percentage of nuclear IN-mCherry complexes, as an indicator of nuclear import, was calculated per cell and is indicated at the top of the graph, where each

(Continued on next page)

TABLE 1 Characteristics of IN-mCherry and CA-eGFP complexes in HeLa P4 cells at 6 h postinfection[a]

		Cytoplasm			Nuclear envelope			Nucleus		
Protein(s)	Virus	Intensity (AU)	No. (%) complexes/cell	*n*	Intensity (AU)	No. (%) complexes/cell	*n*	Intensity (AU)	No. (%) complexes/cell	*n*
IN-mCherry	WT-mCh	0.741 ± 0.821	28.00 ± 10.75 (68)	1,121	0.546 ± 0.547	10.00 ± 5.50 (25)	421	0.463 ± 0.191	2.00 ± 2.37 (6)	99
	CA-eGFP 1:2	0.796 ± 0.819	25.50 ± 10.06 (74)	1,194	0.520 ± 0.492	7.00 ± 4.74 (23)	323	0.374 ± 0.164	0.50 ± 1.57 (3)	50
	CA-eGFP 1:10	0.994 ± 1.184	35.00 ± 12.48 (70)	1,049	0.692 ± 0.694	11.50 ± 4.98 (23)	340	0.513 ± 0.252	2.50 ± 3.12 (7)	99
CA-eGFP	CA-eGFP 1:2	0.314 ± 0.271	15.50 ± 7.94 (41)	612	0.275 ± 0.177	16.00 ± 10.56 (41)	252	0.279 ± 0.178	6.00 ± 5.35 (18)	264
	CA-eGFP 1:10	0.348 ± 0.272	15.00 ± 7.46 (38)	469	0.260 ± 0.197	19.00 ± 7.44 (40)	492	0.282 ± 0.186	9.50 ± 6.63 (22)	302
IN-mCherry+ CA-eGFP	CA-eGFP 1:2		6.00 ± 4.71 (78)	250		1.00 ± 1.18 (12)	52		0.00 ± 0.86 (10)	12
	CA-eGFP 1:10		6.50 ± 4.59 (70)	198		2.00 ± 2.05 (21)	58		0.00 ± 0.50 (9)	6

[a]The table refers to Fig. 7. HeLa P4 cells were infected with single- or double-labelled recombinant virions and fixed 6 h postinfection. Viral complexes were identified and fitted to a 2D Gaussian by in-house Matlab routines. Based on nuclear lamina staining, the complexes were assigned as localizing in the cytoplasm, at the nuclear envelope, or in the nucleus. Shown are fluorescence intensities of identified complexes (in arbitrary units [AU]) and numbers of complexes per cell. All values are plotted as the medians ± standard deviations. For both IN-mCherry and CA-eGFP complexes, the percentage of total complexes localizing in a specific intracellular compartment (cytoplasm, nuclear envelope, or nucleus) is shown as percentage in brackets. *n*, total number of viral complexes identified in a subcellular compartment (cytoplasm, nuclear envelope, or nucleus). Data are derived from one representative of $n = 2$ experiments. Numbers and fluorescence intensities of all identified IN-mCherry (top) and CA-eGFP (middle) complexes in infected HeLa P4 cells. (bottom) Numbers of complexes containing both IN-mCherry and CA-eGFP in infected HeLa P4 cells. In parentheses, percentages of double-labelled complexes per compartment (cytoplasm, nuclear envelope, or nucleus) are shown as the proportion of total double-labelled complexes.

nuclear envelope (Fig. 7I). Most capsid complexes are probably associated with the nonfunctional viral core remnants resulting from uncoating and the release of IN-mCherry-labelled PICs. At 6 h postinfection, 15% of labelled integrase complexes at the nuclear envelope still contained CA-eGFP, which may point to PICs docked at the NE. The remaining IN-mCherry complexes docked at the NE are likely derived from either completely uncoated complexes or those containing unlabelled capsid. We previously demonstrated by fluorescence microscopy of eGFP-IN-labelled virus that almost one-half of IN molecules dissociate at this stage, explaining the presence of eGFP-IN outside the nucleus (41). Only 3% of CA-eGFP complexes in the nucleus contained IN-mCherry even though the labelling of IN is more efficient. The modest particle CA-eGFP labelling efficiency of 25% to 30% may contribute to an apparently low extent of nuclear CA-eGFP and IN-mCherry colocalization. The data indicate that dissociation of CA-eGFP from IN-mCherry complexes likely occurs at the NE.

As indicated by a relatively high (20%) percentage of CA-eGFP complexes in the nucleus, it is possible that CA-eGFP complexes are imported into the nucleus either alone or in association with viral PICs but quickly dissociate from them upon nuclear entry. Either way, the presence of free nuclear CA-eGFP implies that CA may play a role unrelated to integration. Alternatively, CA-eGFP dissociated from the PIC may be degraded in the nuclear proteasome.

Control experiments confirmed that the fluorescent complexes detected were derived from fusion competent viruses (Fig. 8). When we used virus-like particles without VSV-G envelope in parallel with enveloped viruses to transduce HeLa P4 cells, 2- to 10-fold fewer IN-mCherry and CA-eGFP complexes were observed in the cytoplasm and at the NE, and no complexes were detected in the nucleus (Fig. 8 and

FIG 7 Legend (Continued)
value represents percentage mean ± standard error of the mean (SEM). Statistical significance was determined by the Mann-Whitney test. *, $P < 0.05$; n.s., not significant. (C) Fluorescence intensities of IN-mCherry complexes in each subcellular compartment (cytosol, nuclear envelope, and nucleus). (D) Intracellular distributions of CA-eGFP-labelled complexes after transduction of HeLa P4 cells with single- (WT-mCh) or double-labelled (CA-eGFP 1:2 and CA-eGFP 1:10) virions. (E) Fluorescence intensities of CA-eGFP complexes in transduced cells, shown for each subcellular compartment (cytosol, nuclear envelope, and nucleus). (F) Percentages of CA-eGFP complexes (relative to total intracellular CA-eGFP complex numbers) with high eGFP fluorescence intensity. (G) Intracellular distribution of IN-mCherry+CA-eGFP labelled complexes upon transduction of HeLa P4 cells with single- (WT-mCh) or double-labelled (CA-eGFP 1:2 and CA-eGFP 1:10) virions. Fractions of IN-mCherry (H) or CA-eGFP (I) complexes that belong to the colocalizing complexes (containing both fluorophores) were calculated as the number of colocalizing complexes divided by the number of total IN-mCherry or CA-eGFP PICs per cell. Values are expressed as means ± SDs.

TABLE 2 Overview of numbers of nuclear complexes containing either one (IN-mCherry only, CA-eGFP only) or both (IN-mCherry+CA-eGFP) fluorescent labels

Virus	No. of nuclear complexes/cell[a]		
	IN-mCherry only	CA-eGFP only	IN-mCherry+CA-eGFP
CA-eGFP 1:2	0.50 ± 1.57	7.00 ± 4.93	0.00 ± 0.86
CA-eGFP 1:10	6.00 ± 3.09	9.00 ± 6.57	0.00 ± 0.50

[a]All values are plotted as medians ± standard deviations.

Table 3). The data were consistent regardless of the time of cell fixation (1.5 h or 6 h postinfection) (Fig. 8A and B, respectively).

For further experiments, we focused on CA-eGFP 1:10 particles, since CA-eGFP 1:2 displayed a partially defective nuclear import of IN-mCherry-labelled PICs (Fig. 7A) and impaired transduction efficiency.

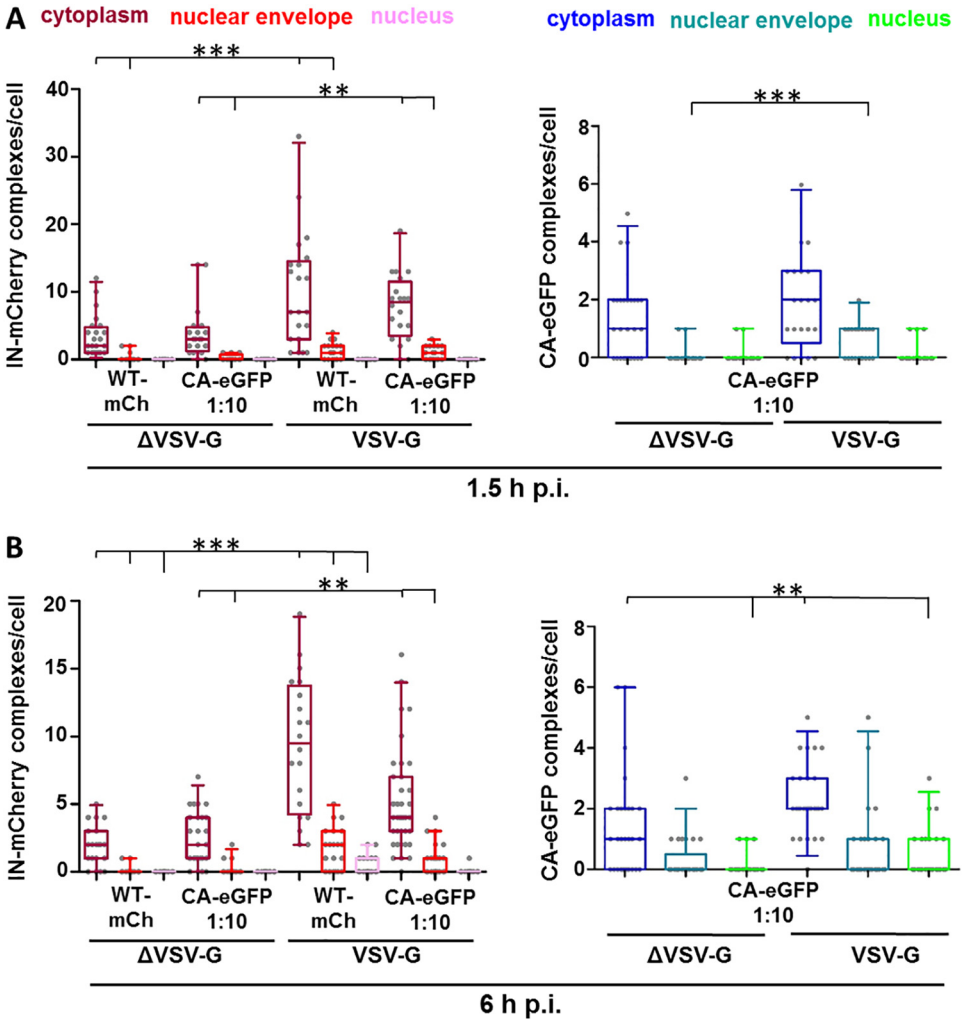

FIG 8 Fluorescent viral complexes are derived from fusion-competent virus particles. Recombinant virus particles or virus-like particles (VLPs) were produced by transient transfection of the HIV-1 pNL4-3.Luc.R-E- vector and pVpr-IN-mCherry, as described in Materials and Methods, with or without the VSV-G-encoding construct, respectively. Same virus particle and VLP amounts (as determined by p24 ELISA) were used to synchronously transduce HeLa P4 cells, which were fixed and immunostained with nuclear lamin antibodies at 1.5 h (A) or 6 h (B) posttransduction. Viruses containing IN-mCherry (WT-mCh) or IN-mCherry and CA-eGFP (CA-eGFP 1:10) are annotated by VSV-G label, whereas the corresponding VLPs are indicated by ΔVSV-G. The numbers of IN-mCherry or CA-eGFP complexes per cell are plotted in 5% to 95% box-and-whisker plots, where the line inside the box represents the median and whiskers represent the outliers. Groups were compared within the same intracellular compartment (e.g., cytosol WT-mCh VLP versus cytosol WT-mCh) and statistical significance was determined by the Mann-Whitney test. **, $P < 0.005$; ***, $P < 0.001$. Lack of annotation represents no statistical significance found between groups. Data are derived from one of $n \geq 2$ independent experiments.

TABLE 3 Numbers of fluorescent complexes in HeLa P4 cells transduced with virus-like particles or enveloped viruses[a]

		No. of complexes/cell							
		IN-mCherry				CA-eGFP			
Time (h)	Virus/VLP	Cytoplasm	Nuclear envelope	Nucleus	*n*	Cytoplasm	Nuclear envelope	Nucleus	*n*
1.5	WT-mCh VLP	2.00 ± 3.07	0.00 ± 0.59	0.00 ± 0.00	85				
	CA-eGFP VLP	3.00 ± 3.88	0.00 ± 0.44	0.00 ± 0.00	83	1.00 ± 1.38	0.00 ± 0.26	0.00 ± 0.26	40
	WT-mCh	7.00 ± 8.40	1.00 ± 1.20	0.00 ± 0.00	242				
	CA-eGFP	8.50 ± 4.90	1.00 ± 1.92	0.00 ± 0.00	175	2.00 ± 1.62	1.00 ± 0.60	0.00 ± 0.36	54
6	WT-mCh VLP	2.00 ± 1.50	0.00 ± 0.31	0.00 ± 0.00	41				
	CA-eGFP VLP	2.00 ± 2.00	0.00 ± 0.47	0.00 ± 0.00	67	1.00 ± 1.66	0.00 ± 0.66	0.00 ± 0.31	52
	WT-mCh	9.50 ± 5.02	2.00 ± 1.55	0.00 ± 0.69	230				
	CA-eGFP	4.00 ± 3.66	0.00 ± 0.99	0.00 ± 0.16	222	2.00 ± 1.15	0.00 ± 1.25	0.00 ± 0.79	84

[a]Recombinant virus particles or virus-like particles (VLPs) were produced by transient transfection of the HIV-1 vector system, as described in Materials and Methods, with or without the VSV-G-encoding construct, respectively. Viruses and VLPs were purified and concentrated, and particle release was assessed by p24 ELISA. Identical particle amounts (determined by p24 ELISA) were used to synchronously transduce HeLa P4 cells, which were fixed and immunostained with nuclear lamin antibodies at 1.5 h (top) or 6 h (bottom) posttransduction. Viruses containing IN-mCherry (WT-mCh) or IN-mCherry and CA-eGFP (CA-eGFP 1:10) are annotated according to their label, whereas the corresponding VLPs are indicated as VLP next to the label name. The complex numbers are shown per intracellular compartment in which they were found (cytosol, nuclear envelope, or nucleus), based on lamin staining. The values shown represent medians ± standard deviations. *n*, the total number of complexes from which data are derived.

IN-mCherry- and CA-eGFP-labelled complexes belong to a functional virus pool. In order to confirm that our approach ensures labelling of functional particles, we investigated the distribution of fluorescent viral complexes after treatment with PF74, a capsid-binding HIV-1 inhibitor (Fig. 9 and 10). We transduced HeLa P4 cells with single- or double-labelled virions in the presence of either dimethyl sulfoxide (DMSO; vehicle control) or PF74 (2 μM and 10 μM) (Fig. 9 and 10). The inhibitory effect of PF74 was tested at both early (1.5 h) and late (6 h) time points postinfection.

At 1.5 h posttransduction, PF74 did not exhibit any influence on the intracellular distribution of IN-mCherry-containing complexes (Fig. 9B and Table 4). While the lower (2 μM) PF74 concentration was not expected to alter IN-mCherry distribution, it was somewhat surprising to observe no effect on the presence of IN-mCherry complexes at the nuclear envelope in the presence of 10 μM PF74. However, this may be a sensitivity issue, as only low numbers of IN-mCherry PICs were observed at the NE soon after infection.

We next analyzed early effects of PF74 on CA-eGFP-containing complexes. In the presence of the DMSO control, docking to the nuclear envelope and nuclear import were observed for CA-eGFP complexes as early as 1.5 h after infection (Fig. 9C). In contrast to that for IN-mCherry, labelled capsid complexes were unable to dock at the nuclear envelope in the presence of a high (10 μM) PF74 concentration, and their nuclear import was blocked by both 2 μM and 10 μM PF74 (Fig. 9C and Table 4). These data agree with previous studies describing capsid perturbation and inhibition of nuclear import by PF74 (23, 33, 41, 47). Importantly, the inhibition of CA-eGFP docking to the NE by 10 μM PF74 indicates that these complexes are part of a functional virion pool.

We next assessed PF74 inhibition at 6 h posttransduction (Fig. 9D and E and Table 5). The intracellular distribution of CA-eGFP complexes in the presence of DMSO was slightly different from that in the initial experiment, as the percentage of CA-eGFP in the nucleus was increased. However, the overall CA-eGFP distribution was reproducible between experiments. Two micromolar PF74 potently inhibited nuclear import of both IN-mCherry- and CA-eGFP-containing complexes (Fig. 9D and E, respectively; Table 5), and 10 μM PF74 abolished the localization of IN-mCherry and CA-eGFP PICs at the nuclear envelope (Fig. 9D and E; Table 5). Decreased complex numbers detected under a high PF74 concentration agree with the capsid destabilizing effect of this inhibitor concentration (32).

In addition to the absolute numbers of fluorescent viral complexes, we also probed their content in the absence versus the presence of inhibitor (Fig. 10; Tables 4 and 5). At 1.5 h postinfection, 10 μM induced a small yet statistically significant increase in

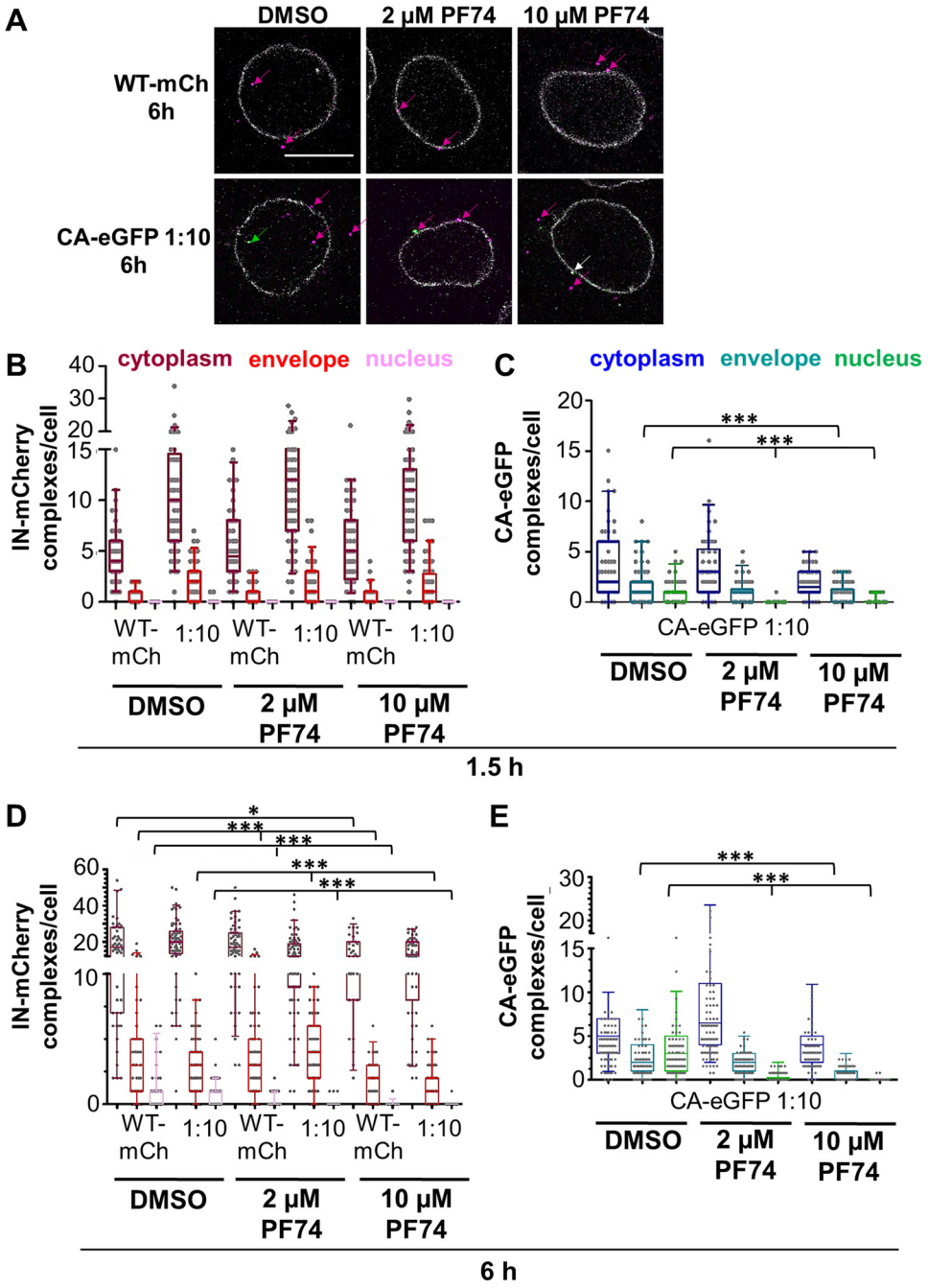

FIG 9 PF74 inhibits nuclear import of IN-mCherry and CA-eGFP complexes. HeLa P4 cells were infected with single- (WT-mCh) or double (1:10)-labelled virions in the presence of DMSO or increasing PF74 concentrations (2 μM or 10 μM) and fixed at 1.5 h or 6 h postinfection. Viral complexes were localized and fitted to a 2D Gaussian distribution by the published in-house Matlab routines. (A) Representative images of transduced HeLa P4 cells fixed 6 h postinfection. Nuclear lamina (defined as shown in Fig. 7A) and viral complexes are indicated in corresponding colors (lamina, white; IN-mCherry, magenta; and CA-eGFP, green). Complexes containing only IN-mCherry or CA-eGFP are indicated by magenta or green arrows, respectively. Complex containing both fluorophores is indicated by a white arrow. Scale bar, 10 μm. (B to E) Data are grouped according to the virus used (WT-mCh, single IN-mCherry-labelled particles; CA-eGFP 1:10 or 1:10, double IN-mCherry+CA-eGFP-labelled virus particles) and to the intracellular compartment (cytoplasm, nuclear envelope, and nucleus) in which the complexes were found. Data are presented in box-and-whisker plots, with the whiskers representing standard deviations, the boxes representing the mean values, and the lines representing the medians. Data represent averages from $n = 2$ independent experiments. Statistically significant differences in PIC numbers were analyzed by the Mann-Whitney test. *, $P < 0.05$; ***, $P < 0.001$. Lack of significance annotation indicates no statistical difference between the samples. Numbers of intracellular IN-mCherry-containing complexes at 1.5 h (B) and 6 h (D) postinfection. Numbers of intracellular CA-eGFP-containing complexes at 1.5 h (C) and 6 h (E) postinfection.

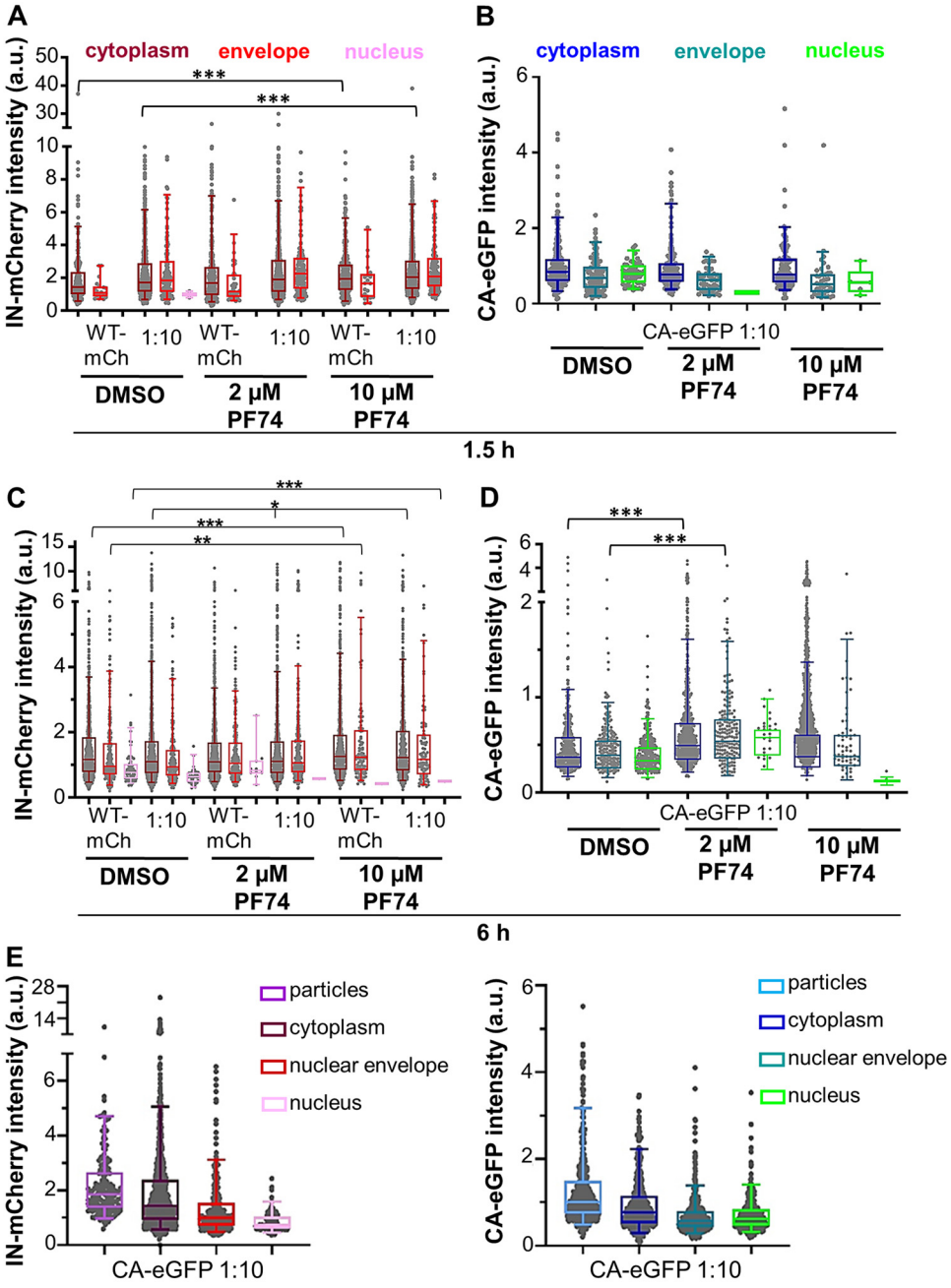

F

IN-mCherry				CA-eGFP			
particles	cytoplasm	nuclear envelope	nucleus	particles	cytoplasm	nuclear envelope	nucleus
1.847 ± 1.292	1.435 ± 1.710	0.999 ± 1.002	0.741 ± 0.364	1.009 ± 0.833	0.770 ± 0.601	0.574 ± 0.435	0.623 ± 0.412

FIG 10 Fluorescent complex intensities under DMSO or PF74 treatment at 1.5 h or 6 h posttransduction. HeLa P4 cells were transduced with IN-mCherry (WT-mCh)- or IN-mCherry+CA-eGFP (CA-eGFP 1:10)-labelled viruses and fixed at 1.5 h or 6 h posttransduction. Transduction was performed in the presence of DMSO or two different PF74 concentrations (2 μM or 10 μM). Viral complexes were identified and characterized using in-house Matlab routines. Integrated fluorescence intensities of single viral complexes were plotted in 5% to 95% box-and-whisker plots (with features as described) and are shown for 1.5 h (A and B) or 6 h (C and D) postinfection. Data are averages from $n = 2$ independent experiments. Statistical analysis of intensity differences was done by the Kruskal-Wallis test with unequal variance. *, $P < 0.05$; **, $P < 0.01$; ***, $P < 0.0001$. The lack of significance annotation indicates no statistical

(Continued on next page)

TABLE 4 Characteristics of IN-mCherry and CA-eGFP complexes in HeLa P4 cells 1.5 h postinfection[a]

Treatment	Virus	No. of complexes/cell			Intensity (AU)			n^b
		Cytoplasm	Nuclear envelope	Nucleus	Cytoplasm	Nuclear envelope	Nucleus	
IN-mCherry								
DMSO	WT-mCh	4.00 ± 3.19	0.00 ± 0.63	NV[c]	1.431 ± 2.650	1.080 ± 0.604	NV	283
	CA-eGFP 1:10	10.00 ± 6.49	2.00 ± 1.77	0.00 ± 0.16	1.708 ± 1.884	1.839 ± 2.240	0.984 ± 0.277	918
2 μM PF74	WT-mCh	4.50 ± 3.66	0.00 ± 0.84	NV	1.679 ± 2.697	1.156 ± 1.267	NV	381
	CA-eGFP 1:10	12.00 ± 6.02	1.00 ± 1.95	NV	1.890 ± 2.534	2.246 ± 2.141	NV	1,009
10 μM PF74	WT-mCh	5.00 ± 4.03	0.00 ± 0.78	NV	1.927 ± 1.618	1.654 ± 1.171	NV	346
	CA-eGFP 1:10	11.00 ± 5.69	1.00 ± 1.94	NV	2.041 ± 2.324	2.077 ± 2.437	NV	997
CA-eGFP								
DMSO	CA-eGFP 1:10	2.00 ± 3.29	1.00 ± 1.85	0.00 ± 1.14	0.839 ± 0.648	0.682 ± 0.453	0.786 ± 0.292	380
2 μM PF74		3.00 ± 3.17	1.00 ± 1.19	0.00 ± 0.15	0.775 ± 0.640	0.620 ± 0.313	0.296 ± 0.000	209
10 μM PF74		1.50 ± 1.39	0.00 ± 1.06	0.00 ± 0.29	0.774 ± 0.722	0.512 ± 0.644	0.561 ± 0.343	152

[a]HeLa P4 cells were transduced with single- (WT-mCh) or double-labelled (CA-eGFP) virus particles, in the presence of either DMSO or PF74 (2 μM or 10 μM) and fixed 1.5 h postinfection. Fluorescent virus complexes were localized and fitted with a 2D Gaussian curve. Integrated intensity was calculated in each z-section. The experiment was performed twice, and the means of all data are shown. The data were collected from 50 to 60 cells corresponding to approximately 500 IN-mCherry and 300 CA-eGFP complexes detected in total. The complex numbers are shown per intracellular compartment in which they were found (cytosol, nuclear envelope, or nucleus), based on lamin staining. The values shown represent medians ± standard deviations.

[b]*n*, the total number of complexes from which data are derived.

[c]NV, no virus.

fluorescence intensity of cytoplasmic IN-mCherry complexes (1.35- and 1.19-fold increases for WT-mCh and CA-eGFP 1:10 infections, respectively) (Fig. 10A). There was no significant change in the content of CA-eGFP complexes (Fig. 10B). At 6 h postinfection, treatment with 10 μM PF74 also induced increased fluorescence intensities of cytoplasmic and NE IN-mCherry complexes (Fig. 10C). For complexes detected under the WT-mCh condition, fluorescence intensity was 0.95-fold decreased in the cytosol but 1.24-fold increased at the nuclear envelope. For the CA-eGFP 1:10 condition, fluorescence intensities of IN-mCherry were 1.12- and 1.24-fold increased in the cytoplasm and at the NE, respectively, under the same PF74 treatment. PF74 is not expected to directly affect IN-mCherry content of the viral PICs, and the effects of a high PF74 concentration, although statistically significant, are discrete. One possibility is that IN-mCherry fluorescence is detected more efficiently when the cone is destabilized by high PF74. As for the CA-eGFP intensity profiles, the data should be interpreted cautiously due to the low numbers of encapsidated CA-eGFP monomers. The CA-eGFP content in the viral complexes was unaffected by PF74 treatment at 1.5 h postinfection (Fig. 10B). In contrast, the CA-eGFP intensity was significantly increased by 2 μM PF74 for cytoplasmic and NE complexes (1.33- and 1.37-fold increases, respectively) detected at 6 h postinfection (Fig. 10D). These data agree with previous findings on capsid stabilization effects of low PF74 concentrations, whereby CA-eGFP fluorescence possibly increases due to aborted or delayed uncoating and associated loss of some CA-eGFP molecules. The finding that 10 μM PF74 does not radically influence the CA-eGFP content (Fig. 10B and D) further supports the hypothesis that this fusion protein is not part of the core surface and resides solely inside the core and not in a hexameric form.

As an additional confirmation that the visualized complexes originate from fusion-competent particles, we compared fluorescence intensities of intact viruses spotted on

FIG 10 Legend (Continued)
significance. (E) Comparison of IN-mCherry and CA-eGFP intensities in intact particles versus intracellular virus complexes. Double-labelled viruses were produced as in Materials and Methods. The particles were spotted on microscopic glass coverslips, fixed, and immunostained with the p24 antibody to detect single virus particles. The same virus prep was used in parallel to infect HeLa P4 cells. Fixed viruses and infected cells were imaged in the same experiment and under the same conditions. Fluorescent complexes were identified and characterized using an in-house Matlab routine. The spotted viruses are denoted as "particles," and intracellular virus complexes are denoted according to the compartment (cytoplasm, nuclear envelope, and nucleus). Fluorescence intensities of viral complexes were measured for each complex and are shown for both CA-eGFP and IN-mCherry. The complex intensities are plotted into 5% to 95% box-and-whisker plots, where the lines in the boxes represent the median numbers and the whiskers represent outliers. (F) Median intensities ± standard deviations for all identified complexes are shown in the table. Shown are the data from one representative of $n = 2$ experiments.

TABLE 5 Characteristics of IN-mCherry and CA-eGFP complexes in HeLa P4 cells 6 h postinfection[a]

Treatment	Virus	No. of complexes/cell			Intensity (AU)			n^b
		Cytoplasm	Nuclear envelope	Nucleus	Cytoplasm	Nuclear envelope	Nucleus	
IN-mCherry								
DMSO	WT-mCh	14.00 ± 10.95	3.00 ± 3.81	0.00 ± 0.86	1.164 ± 1.147	0.956 ± 1.081	0.768 ± 0.495	1,572
	CA-eGFP 1:10	20.00 ± 10.34	3.00 ± 2.38	0.00 ± 0.90	1.094 ± 1.380	0.936 ± 0.974	0.633 ± 0.248	1,775
2 μM PF74	WT-mCh	12.50 ± 10.17	2.00 ± 3.38	0.00 ± 0.34	1.092 ± 1.003	1.046 ± 0.899	0.828 ± 0.579	1,710
	CA-eGFP 1:10	12.00 ± 9.02	4.00 ± 2.48	0.00 ± 0.19	1.107 ± 1.280	1.060 ± 1.411	0.578 ± 0.000	1,438
10 μM PF74	WT-mCh	11.00 ± 6.92	1.00 ± 1.30	0.00 ± 0.12	1.257 ± 1.473	1.231 ± 1.640	0.422 ± 0.000	983
	CA-eGFP 1:10	13.00 ± 7.33	1.00 ± 1.47	0.00 ± 0.13	1.224 ± 1.381	1.165 ± 1.296	0.499 ± 0.000	886
CA-eGFP								
DMSO	CA-eGFP	5.00 ± 3.25	2.00 ± 2.34	3.00 ± 3.63	0.370 ± 0.427	0.391 ± 0.304	0.333 ± 0.202	866
2 μM PF74		6.50 ± 8.32	2.00 ± 1.55	0.00 ± 0.61	0.494 ± 0.478	0.538 ± 0.447	0.575 ± 0.201	920
10 μM PF74		4.00 ± 2.74	1.00 ± 0.90	0.00 ± 0.18	0.376 ± 0.411	0.378 ± 0.491	0.120 ± 0.060	311

[a]The table refers to Fig. 9 HeLa P4 cells were transduced with single- (WT-mCh) or double-labelled (CA-eGFP) virus particles in the presence of either DMSO or PF74 (2 μM or 10 μM) and fixed 6 h postinfection. Fluorescent virus complexes were localized and fitted with a 2D Gaussian curve. Integrated intensity was calculated in each z-section. The experiment was performed twice, and the means from all data are shown. The data were collected from 50 to 60 cells corresponding to approximately 1,000 IN-mCherry and 600 CA-eGFP complexes detected in total. The complex numbers are shown per intracellular compartment in which they were found (cytosol, nuclear envelope, or nucleus), based on lamin staining. The values shown represent medians ± standard deviations.
[b]*n*, the total number of complexes from which data are derived.

coverslips and postfusion viral complexes, identified in the target cells (Fig. 10E and F). The fluorescence intensities of both cytoplasmic IN-mCherry and CA-eGFP complexes were lower than for the intact viruses used for transduction and imaged under the same conditions. We hence conclude that the observed and analyzed viral complexes were derived from fusion-competent virus particles.

To corroborate our imaging data, we performed transduction experiments in the presence of DMSO or PF74 to quantify luciferase reporter gene expression and viral DNA species in infected HeLa P4 cells (Fig. 11). To compare the transduction efficiency of unlabelled, single-, and dually labelled viruses, we transduced HeLa P4 cells in parallel with different dilutions of virus after initial normalization for p24. As shown in Fig. 11A, transduction efficiencies were comparable between all viruses, confirming that IN-mCherry and/or CA-eGFP colabelling do not drastically interfere with transduction. PF74 inhibited transduction of all viruses in a concentration-dependent manner (Fig. 11A). We also quantified total viral DNA after normalization for cellular genomic DNA content (Fig. 11B). Viral integration was evaluated only in the absence of inhibitor, and integration rates (measured by the Gag gene levels in the cellular genomic DNA) were comparable for all viruses (Fig. 11B).

Presence of CA-eGFP in the nucleus. Previously, our lab showed that IN-FP labelling enables visualization of functional viral complexes in target cells (41). A hallmark feature of IN-FP functionality is the observed accumulation of fluorescent IN complexes in the nucleus upon addition of the integrase strand transfer inhibitor raltegravir (RAL) (41), which was recently confirmed in an independent study (18). Here, we asked how RAL influences intracellular distributions of CA-eGFP complexes at 6 h postinfection. We first analyzed IN-mCherry distribution profiles and detected that, like IN-eGFP, the mCherry-tagged IN complexes accumulated in the nucleus upon integrase inhibition (Fig. 12A). This accumulation was observed as a significantly increased percentage of nuclear complexes compared to the total number of intracellular IN-mCherry complexes. The percentage of CA-eGFP complexes in the nucleus was unaffected by RAL addition (Fig. 12B). Next, we quantified the percentages of single- (CA-eGFP or IN-mCherry) and double-labelled (IN-mCherry+CA-eGFP) complexes in the nuclei of cells infected with double-labelled virions (CA-eGFP 1:10) (Fig. 12C to E). Interestingly, inhibiting integration resulted in distinct effects on double-labelled viral complexes. When plotting percentages of nuclear IN-mCherry complexes per cell (Fig. 12C) in cells infected with double-labelled virions, we observed that the percentage of IN-mCherry-only-containing complexes was increased upon RAL treatment, while there was no effect on the accumulation of double-labelled complexes (Fig. 12C and E). We

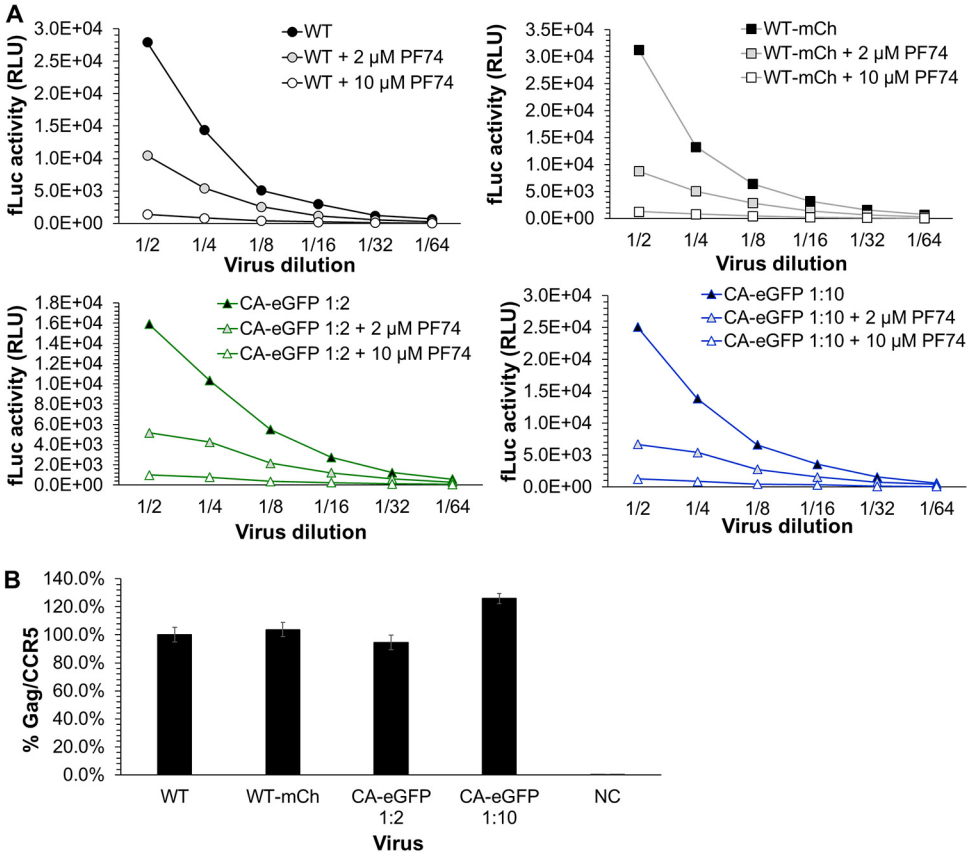

FIG 11 Transduction efficiency and quantification of viral DNA upon transduction of HeLa P4 cells with unlabelled, single-, and dually labelled viruses (supplementary to Fig. 3 and 6). Recombinant VSV-G-pseudotyped viruses were produced and concentrated as described in Materials and Methods. For production of unlabelled particles (WT), only the parental pNL4-3.Luc.R-E- vector was used in combination with the pLP-VSV-G plasmid. Single- (WT-mCh) and dually labelled particles were produced as described above, with two different ratios (1:2 and 1:10) pf CA-eGFP coding vector to the parental pNL4-3.Luc.R-E- plasmid in the case of dually labelled virions (ratios indicated in figure keys). (A) HeLa P4 cells were seeded for transduction as described in Materials and Methods. The following day, the cells were pretreated with DMSO or 2 μM or 10 μM PF74 prior to transduction with different dilutions of virus (indicated on the *x* axes). All transductions were performed in parallel in the same experiment, using virus supernatants produced in parallel. The virus dilutions were made starting from RT-normalized supernatants. Transduction efficiencies were determined by fLuc activity, normalized for total protein content (BCA). Data are plotted as the means ± SDs from biological triplicates. (B) Quantification of total viral DNA in transduced HeLa cells 7 days posttransduction. Genomic DNA was extracted from transduced cells, and viral DNA was quantified by means of Gag-specific qPCR. Viral DNA copies were normalized for cellular input via the CCR5-specific qPCR. Viral DNA levels in cells transduced with unlabelled (WT) virus were arbitrarily set to 100%, and all other transduced samples (labelled according to the virus used) were plotted relative to the WT. Data are plotted as the means ± SDs from biological duplicates.

then plotted the percentages of CA-eGFP complexes containing either only the tagged CA or both labelled CA and IN (Fig. 12D and E). We observed no significant changes in the percentages of either complex species relative to the total number of intracellular CA-eGFP complexes. These data indicate either that the majority of CA-eGFP-containing complexes may not belong to integration-competent PICs or that capsid (and CA-eGFP) must dissociate prior to the generation of integration-competent PICs. In agreement with previous studies, it is possible that the PIC-associated CA and CA-eGFP influence nuclear import, migration, and/or targeting of PICs inside the nucleus, but that they are likely not involved in the integration reaction.

DISCUSSION

In this study, we describe an original HIV-1 capsid protein labelling strategy using CA-eGFP. Using an extended confocal imaging platform for HIV-1, we show that (i) small amounts of eGFP-labelled CA protein are incorporated into virus particles without

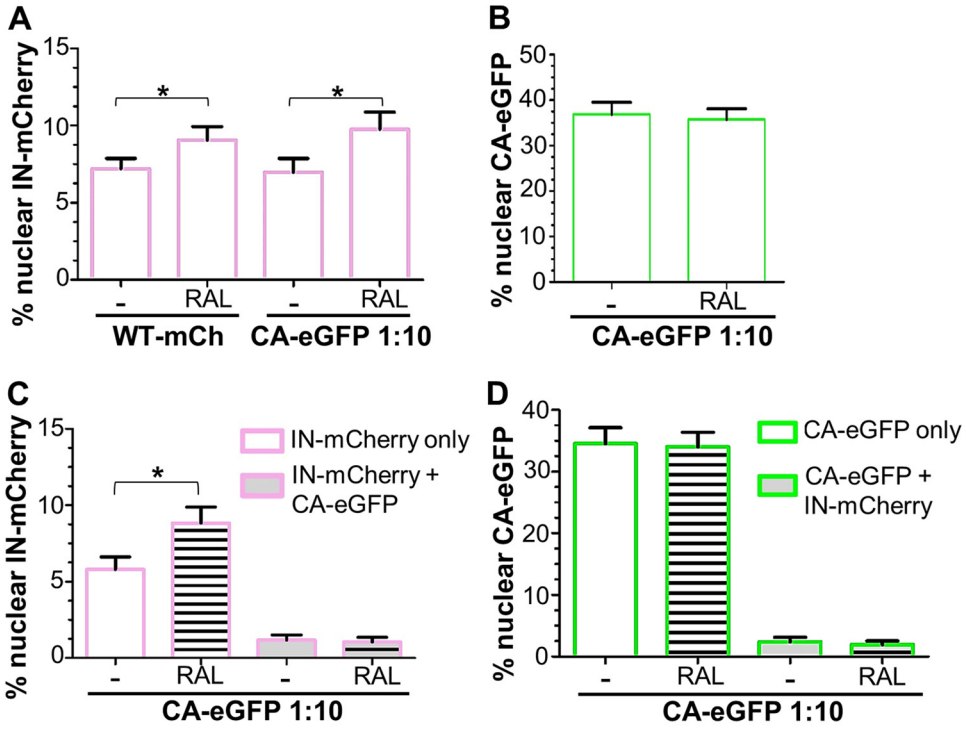

E

	% nuclear IN-mCherry complexes		% nuclear CA-eGFP complexes	
	IN-mCherry	IN-mCherry + CA-eGFP	CA-eGFP	CA-eGFP + IN-mCherry
DMSO	5.81 ± 0.81	1.17 ± 0.34	34.55 ± 2.56	2.37 ± 0.76
RAL	8.83 ± 1.06	1.04 ± 0.31	34.03 ± 2.35	1.97 ± 0.55

FIG 12 Impact of integrase inhibition on CA-eGFP and IN-mCherry complexes in the nucleus. HeLa P4 cells were transduced with IN-mCherry (WT-mCh) or IN-mCherry+CA-eGFP (CA-eGFP 1:10) viruses in the presence of DMSO or 0.6 μM RAL. Cells were fixed at 6 h posttransduction, the nuclear lamina was immunostained, and viral IN-mCherry and CA-eGFP complexes were identified and localized using the described in-house Matlab routines (see Materials and Methods). Percentages of IN-mCherry (A), CA-eGFP (B), and double-labelled complexes (CA-eGFP+IN-mCherry) (C and D) were determined out of the total complex numbers per cell, and values are plotted as means ± SEMs. For cells infected with double-labelled virions (CA-eGFP 1:10), percentages of singly (IN-mCherry only; CA-eGFP-only) and double-labelled complexes (IN-mCherry+CA-eGFP) are plotted separately. Data are averages from $n = 2$ independent experiments. *, $P < 0.05$ obtained with a Mann-Whitney test. Lack of statistical significance is not indicated. (E) Summary table indicating the proportion of nuclear complexes out of total CA-eGFP and IN-mCherry complexes. Values are represented as means ± SEMs. Categories "IN-mCherry and CA-eGFP" refer to the nuclear PICs containing only the respective label; double-labelled nuclear PICs are designated "IN-mCherry+CA-eGFP" and "CA-eGFP+IN-mCherry," depending on whether the percentage of these complexes was calculated relative to the total number of all IN-mCherry- or all CA-eGFP-labelled complexes, respectively.

major interference with viral transduction or nuclear import of IN-mCherry labelled PICs, (ii) CA-eGFP is located inside the viral capsid core, (iii) CA-eGFP-containing virions belong to a functional virus pool, and (iv) nuclear CA-eGFP-containing IN complexes respond differently to integrase inhibitors than complexes without (the labelled) CA. Taken together, these data highlight the validity of our labelling system and the use of CA-eGFP as a direct marker of a functional capsid protein pool.

Following the fate of HIV-1 CA in infected cells has gained increasing interest in recent years, as the possible role of this protein in postuncoating steps attracted much attention and controversy (reviewed in reference 1). Previous studies pointed to important roles for CA in docking of HIV-1 PICs to the NE and their consecutive import into the nucleus (reviewed in reference 1). The CA protein itself was detected in the nucleus, albeit predominantly using immunostaining with specialized protocols (24,

25). Therefore, we opted for developing a direct CA labelling strategy, to allow robust detection of this viral protein in the nucleus and to decipher its intracellular distribution with respect to IN-FP labelled viral PICs.

In our strategy, we produce transduction-competent particles containing an excess of untagged over tagged CA. We postulate that the CA-eGFP protein is located primarily inside mature virus cores. The following lines of evidence support this model. (i) The particles incorporate on average only 2 CA-eGFP monomers per virion (Fig. 5C); (ii) tagged CA molecules are resistant to saponin-mediated membrane stripping *in vitro*, excluding CA-eGFP location between the viral core and membrane (Fig. 6A and B); (iii) fluorescence intensity measurements point to the relatively unaltered CA-eGFP signal from entry to nuclear import, which can be explained by a few CA-eGFP monomers that reside inside the cone and that are therefore unaffected by uncoating (Fig. 7E). We believe that our approach visualizes an insufficiently discussed intraparticle CA population, which is present inside the viral core and associates with the viral PICs during early infection. Of course, at this stage, we cannot exclude that eGFP tagging of CA may have artificially resulted in this CA population. Since CA-eGFP is present only in approximately 25% to 30% of all virus particles (Fig. 5B), we admit that this labelling is less efficient than some previously published approaches, such as binding of CypA-dsRed to viral cores (43) or tC tagging of CA in recombinant virions (36, 37). However, a considerable advantage of using CA-eGFP compared to those approaches is the direct visualization of CA rather than its interacting partner (in the case of CypA-dsRed) or the use of a secondary dye (such as FlAsH, in the case of tC labelling). Additionally, CA-eGFP offers a good alternative to CA immunostaining approaches, which provide a limited and variable visualization of CA in the host cell nucleus and are not suited for live-cell imaging approaches (23–25).

Importantly, CA-eGFP complexes represent functional complexes, as illustrated by the following experiments: (i) the number of CA-eGFP complexes derived from virus-like particles (VLPs) is significantly lower than from enveloped particles and they are deficient for nuclear import (Fig. 8); (ii) PF74 prevents nuclear envelope docking and nuclear import of CA-eGFP complexes in a dose-dependent manner (Fig. 9), consistent with previous findings (23, 34).

While CA-eGFP present within the viral cone cannot be used as a direct label for core uncoating, it may provide a useful tool for labelling and tracking of the functional CA population. Low PF74 concentrations do not cause capsid destabilization (23, 25, 34) but may still perturb the uncoating process and thereby prevent HIV-1 nuclear import. In agreement with this model, 2 μM PF74 blocked the nuclear import of both CA-eGFP and IN-mCherry complexes. Consistently with previous studies, 10 μM PF74 also inhibited docking of both CA-eGFP and IN-mCherry particles at the nuclear envelope, which in turn is consistent with the NE uncoating model (see Fig. 13 for summary). An additional observation that supports this model in our study is the low colocalization rate of IN-mCherry and CA-eGFP at the NE. Even though CA-eGFP may reside within the core, uncoating or a postuncoating CA rearrangement would be required to free it from IN-mCherry. Due to the presence of many free CA-eGFP complexes (approximately 95% of all CA-eGFP complexes) at the NE and in the nucleus, we propose a model in which the majority of labelled capsid and integrase proteins are independently imported into the nucleus and likely perform distinct roles there.

The present data on CA-eGFP distribution largely agree with previous publications, which imply the existence of capsid multimers that persist after uncoating and nuclear import (18, 24, 25). As even from dynamic studies it is unclear which CA rearrangements occur during uncoating (18), these complexes may have been released from PICs together with viral core remnants at the moment of nuclear import. The presence of CA-eGFP in the nucleus is in line with previous findings describing relatively low capsid protein content in the nuclei of infected cells (18, 25). Even though it was previously shown that the intensity of immunostained or otherwise labelled CA complexes is 5- to 10-fold lower than in the cytoplasm (18, 25), it is possible to detect them as clear foci, indicating that nuclear CA exists in a multimeric form.

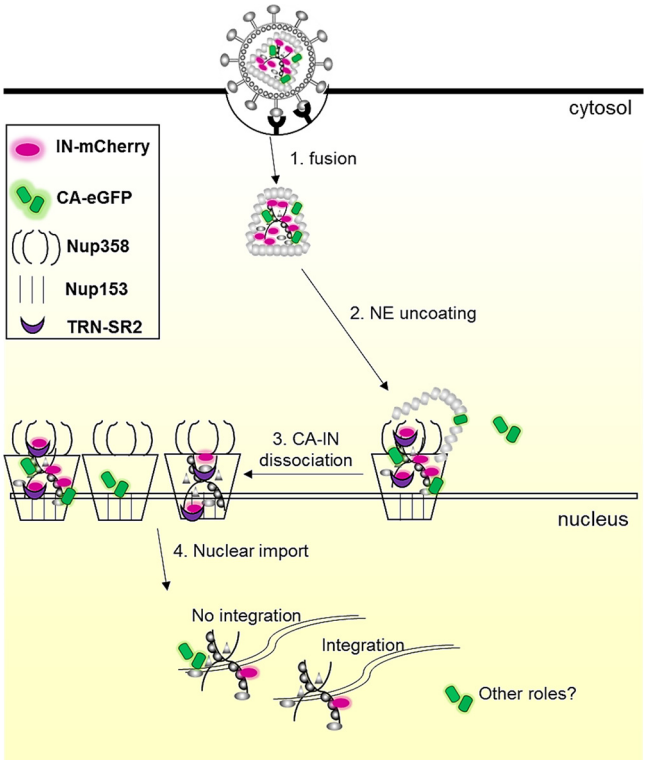

FIG 13 HIV-1 entry model based on CA-eGFP labelling. Double-labelled virions containing IN-mCherry and CA-eGFP enter the cells via fusion. Most CA-eGFP complexes dissociate from IN-mCherry complexes by 6 h postinfection at the NE. CA-eGFP follows three pathways: majority (85%) of CA-eGFP is imported into the nucleus independently of IN-mCherry, a second portion (10%) is imported together with IN, and a third portion remains associated at the nucleopore, possibly as an empty shell (5%). After import of complexes docked at the NE pores, IN-mCherry is associated with integration competent complexes, while the role of nuclear CA-eGFP complexes remains to be elucidated.

Once localized in the nucleus, 97% of CA-eGFP complexes do not contain IN-mCherry and do not seem to participate in integration, as deduced from our RAL experiments (Fig. 12B and D). Accumulation of IN-mCherry complexes under RAL treatment is particularly clear when comparing PICs that contain only labelled IN and those that contain both IN-mCherry and CA-eGFP (Fig. 12C). The percentage of PICs containing only IN significantly increases by approximately 50%, while the population of double-labelled complexes remains unchanged. In contrast to these data, analysis of CA-eGFP-containing nuclear complexes revealed a different phenotype (Fig. 12B and D). No effect was seen on the overall percentage of CA-eGFP complexes (both without and with IN-mCherry) in the nucleus (Fig. 12B and D). Our data indicate that most nuclear CA complexes differ from IN complexes without CA in response to integrase inhibitors, suggesting that the labelled CA complexes do not participate in integration. We believe our data add value to previous studies, mostly due to their quantitative aspect. Previously, Chin and colleagues (24) implied that CA is associated with integration-competent virus complexes in the nucleus, based on the observed stabilization of CA colocalization with vDNA under RAL treatment, but without any detailed quantification. These data were more recently challenged by another study (18), which showed that integration events (marked by IN-eGFP disappearance in the nucleus) did not contain CA in 50% of the cases. Our data thus agree with the latter findings and with a recently published study (28), whereby the primary role of nuclear CA is in traversing the nuclear lamina to allow PICs to reach optimal regions prior to integration.

Our present imaging analysis confirms previous findings on integration-competent PICs in the nucleus (41) but leaves ground for future mechanistic studies. To expand these findings on the role of CA and CA-eGFP inside the nucleus, a time course analysis

of integration-deficient virus and/or mutants not interacting with CPSF6 (such as N74D and A77V) is planned. It will also be interesting to perform integration site analyses of cells transduced with single- and double-labelled viruses. Future live-cell imaging studies will shed further light on these events. Taken together, our capsid labelling system enables tracking of functional virus particles and therefore represents a relevant complementary system to the existing methodologies for further dissecting the role of HIV-1 capsid during early infection.

MATERIALS AND METHODS

Cells. All mammalian cell lines were cultured at 37°C in a humidified atmosphere with 5% CO_2. HeLa P4 (a kind gift from Pierre Charneau, Institut Pasteur, Paris, France) and HEK293T (ATCC CRL-11268) cells were maintained in Dulbecco's modified eagle medium (DMEM; Life Technologies Europe, Merelbeke, Belgium) supplied with 5% (vol/vol) fetal calf serum (FCS), 50 μg/ml gentamicin (Life Technologies), and in the case of HeLa P4, additionally, 500 μg/ml Geneticin (Gibco BRL). The cells were subcultured twice a week.

Recombinant DNA. The pNL4-3.Luc.R-E- construct was obtained through the NIH AIDS Reagent Program (catalog number 3418) from Nathaniel Landau (48). The plasmid pVpr-IN-eGFP was described previously (40), and pVpr-IN-mCherry was constructed by replacing the eGFP gene in pVpr-IN-eGFP with mCherry via BamHI and NotI restriction sites. The linker between IN and the FP is the same in both constructs. pLP-VSV-G was described previously (pLP-VSVG, 646 B; Invitrogen). Two types of tC tags were used for tC tagging of CA: a shorter (CCPGCC, inserted within the CA sequence) and longer (FLNCCPG CCMEP, attached at the N or C terminus of CA) tC tag. Site-directed ligase-independent mutagenesis (SLIM) method (49) was used to introduce the corresponding tC CA tags into pNL4-3.Luc.R-E-. Each primer used in the SLIM approach is annotated by its orientation (forward sense [F] and reverse antisense [R]) and special feature (tailed [t] and short [s]). The pNL4-3.Luc.R-E-based constructs coding for tC-tagged CA variants (thus named pNL4-3.Luc.R-E-tC) and primers used were the following: tC_{4-9} (Ft, TGGTACATCAGGCCATATCACC; Fs, TGTTGTCCCGGGTGTTGCATGGTACATCAGGCCATATCACC; Rt, CACTAT AGGGTAATTTTGGCTGACC; Rs, TGCAACACCCGGGACAACACACTATAGGGTAATTTTGGCTG ACC), tC_{91-95} (Ft, ATGAGAGAACCAAGGGGAAGTG; Fs, TGTTGTCCAGGATGTTGTATGAGAGAACCAAGGGGAAGTG; Rt, AG GCCCTGCATGCACTGG; Rs, ACAACATCCTGGACAACAAGGCCCTGCATGCACTGG), $tC_{120-124}$ (Ft, CAGTAGGA GAAATCTATAAAAGATGG; Fs, TGTTGCCCAGGATGTTGTCCAGTAGGAGAAATCTATAAAAGATGG; Rt, TGTCA TCCATCCTATTTGTTCC; Rs, GACAACATCCTGGGCAACATGTCATCCATCCTATTTGTTCC), $tC_{206-210}$ (Ft, CTAG AAGAAATGATGACAGC; Fs, TGTTGTCCCGGGTGTTGTCTAGAAGAAATGATGACAGC; Rt, CAATGCTTTTAAAA TAGTCTTACAATC; Rs, ACAACACCCGGGACAACACAATGCTTTTAAAATAGTCTTACAATC), tC-CA (N-terminal fusion) (Ft, CCTATAGTGCAGAACCTCCAGG; Fs, CCAATTGTGCAGTTTCTGAATTGTTGTCCCGGGTGTTGTATG GAACCTCCTATAGTGCAGAACCTCCAGG; Rt, GTAATTTTGGCTGACCTGGCTG; Rs, AGGTTCCATACAACACCC GGGACAACAATTCAGAAACTGCACAATTGGGTAATTTTGGCTGACCTGGCTG), and CA-tC (C-terminal fusion) (Ft, GCTGAAGCAATGAGCCAAG; Fs, TTTCTGAATTGTTGTCCCGGGTGTTGTATGGAACCTGCTAGGGTGCTAGC TGAAGCAATGAGCCAAG; Rt, CAAAACTCTTGCTTTATGGCCG; Rs, TAGCACCCTAGCAGGTTCCATACAACACC CGGGACAACAATTCAGAAACAAAACTCTTGCTTTATGGCCG). N- and C-terminal eGFP tagging of CA was achieved by ligating the BamHI/SpeI- and SpeI/ApaI-digested gBlocks (IDT, Leuven) into the pNL4-3.Luc.R-E- backbone, respectively. The construct pNL4-3.Luc.R-E-CA-eGFP (referred to as NL4-3 Luc CA-eGFP) is a modification of the above-described vector though replacing the capsid sequence in the *gag* open reading frame (ORF) with the CA-eGFP fusion sequence.

(i) Full gBlock sequence for eGFP-CA fusion. Italic underlined sequence indicate duplicated protease cleavage site, *italic* sequence indicates eGFP, underlining indicates the GGSGT linker, boldface font designates the N terminus of CA, and boldface font with underlining for ACTAGT indicates SpeI restriction site: GAGTTAATACGACTCACTATAGGGGGATCCGAAGAACTTAGATCATTATATAATACAATAGCAG TCCTCTATTGTGTGCATCAAAGGATAGATGTAAAAGACACCAAGGAAGCCTTAGATAAGATAGAGGAAGAGCAA AACAAAAGTAAGAAAAAGGCTCAGCAAGCAGCAGCTGACACAGGAAACAACAGCCAGGTC*AGCCAAAATTACC CCATCGTACAAAAT*ATGGTGAGCAAGGGCGAGGAGCTGTTCACCGGGGTGGTGCCCATCCTGGTCGAGCTGGACGGC *GACGTAAACGGCCACAAGTTCAGCGTGTCCGGTGAGGGGGAGGGCGACGCAACTTATGGCAAATTGACGCTCAAGTT TATCTGCACCACAGGCAAGCTTCCCGTGCCCTGGCCTACATTGGTGACCACTCTGACTTACGGGGTGCAGTGTTTCAGT AGATATCCCGACCACATGAAGCAGCACGATTTCTTCAAGAGTGCAATGCCCGAAGGTTACGTACAGGAAAGGACTATT TTCTTCAAGGACGATGGTAACTATAAAACTCGGGCGGAGGTGAAATTCGAGGGGGACACGCTGGTAAATCGCATTGA GCTGAAGGGAATCGATTTCAAAGAGGATGGCAATATCCTCGGCCATAAATTGGAATACAACTATAACAGTCATAATGT GTACATTATGGCAGACAAGCAGAAAAACGGGATAAAAGTCAATTTCAAGATTAGACATAACATAGAAGATGGGTCAGT CCAGCTCGCAGATCACTATCAGCAGAACACACCCATTGGGGATGGACCAGTGCTGCTCCCTGACAACCACTACCTGAG CACCCAGTCCGCCCTGAGCAAAGACCCCAACGAGAAGCGCGATCACATGGTCCTGCTGGAGTTCGTGACCGCCGCCG GGATCACTCTCGGCATGGACGAGCTGTACAAG*GGAGGGTCCGGAACA***CCTATAGTGCAGAACCTCCAGGGGCA ATGGTACATCAGGCCATATCACCGCGGACTTTAAATGCATGGGTAAAAGTAGTAGAAGAGAAGGCTTT CAGCCCAGAAGTAATACCCATGTTTTCAGCATTATCAGAAGGAGCCACCCCACAAGACCTAAATACCATG CTAAACACAGTGGGGGGACATCAAGCAGCCATGCAAATGTTAAAAGAGACCATCAATGAGGAAGCTGCA GAATGGGATAGATTGCATCCAGTGCATGCAGGGCCTATTGCACCAGGCCAGATGAGAGAACCAAGGGGA AGTGACATAGCAGGAACT**ACTAGT**CCGCTGAGCAATAACTAGCCTGA.

(ii) Full gBlock sequence for CA-eGFP fusion. Bold font indicates CA C terminus, boldface font with underling for ACTAGT indicates the SpeI restriction site, boldface font for ACAAGCAT is the mutated BstxI site; underlining indicates DPPVAT linker, and the italic sequence indicates eGFP): GAGTTAATACGACTC

ACTATAGGG**ACTAGT**ACCCTTCAGGAACAAATAGGATGGATGACACATAATCCACCTATCCCAGTAGGAG
AAATCTATAAAAGATGGATAATCCTGGGATTAAACAAAATAGTAAGAATGTATAGCCCTACAAGCATTCT
GGACATAAGACAAGGACCAAAGGAACCCTTTAGAGACTATGTAGACCGATTCTATAAAACTCTAAGAGC
TGAGCAAGCTTCACAAGAGGTAAAAAATTGGATGACAGAAACCTTGTTGGTCCAAAATGCGAACCCAGA
TTGTAAGACTATTTTAAAAGCATTGGGACCAGGAGCGACACTAGAAGAAATGATGACAGCATGTCAGGG
AGTGGGGGGACCCGGCCATAAAGCAAGAGTTTTGGATCCTCCAGTGGCCACC*ATGGTGAGCAAGGGCGAGGA*
GCTGTTCACCGGGGTGGTGCCCATCCTGGTCGAGCTGGACGGCGACGTAAACGGCCACAAGTTCAGCGTGTCCGGTG
AGGGGGAGGGCGACGCAACTTATGGCAAATTGACGCTCAAGTTTATCTGCACCACAGGCAAGCTTCCCGTGCCCTGGC
CTACATTGGTGACCACTCTGACTTACGGGGTGCAGTGTTTCAGTAGATATCCCGACCACATGAAGCAGCACGATTTCTT
CAAGAGTGCAATGCCCGAAGGTTACGTACAGGAAAGGACTATTTTCTTCAAGGACGATGGTAACTATAAAACTCGGGC
GGAGGTGAAATTCGAGGGGGACACGCTGGTAAATCGCATTGAGCTGAAGGGAATCGATTTCAAAGAGGATGGCAATA
TCCTCGGCCATAAATTGGAATACAACTATAACAGTCATAATGTGTACATTATGGCAGACAAGCAGAAAAACGGGATAA
AAGTCAATTTCAAGATTAGACATAACATAGAAGATGGGTCAGTCCAGCTCGCAGATCACTATCAGCAGAACACACCCA
TTGGGGATGGACCAGTGCTGCTCCCTGACAACCACTACCTGAGCACCCAGTCCGCCCTGAGCAAAGACCCCAACGAG
*AAGCGCGATCACATGGTCCTGCTGGAGTTCGTGACCGCCGCCGGGATCACTCTCGGCATGGACGAGCTGTACAAG*GC
CCGGGTACTGGCTGAAGCAATGAGCCAAGTAACAAATCCAGCTACCATAATGATACAGAAAGGCAATTTTAGGA
ACCAAAGAAAGACTGTTAAGTGTTTCAATTGTGGCAAAGAAGGGCACATAGCCAAAAATTGCAGGGCCCCCGCT
GAGCAATAACTAGCCTGA.

Virus particle production. Recombinant, replication-deficient HIV-1 particles were produced by transient transfection of selected plasmids into 293T cells, as described previously (41). The plasmid mixtures consisted of 15 μg NL4-3 Luc-based construct (either pNL4-3.Luc.R-E- only or mixed at 2:1 and 10:1 ratios with pNL4-3 Luc CA-eGFP), 15 μg pVpr-IN-eGFP or pVpr-IN-mCherry, and 5 μg pVSV-G plasmid per 10-cm cell culture dish unless explicitly stated otherwise. For production of unlabelled virus particles, 15 μg of pNL4-3.Luc.R-E- construct was cotransfected with 5 μg of pLP-VSV-G plasmid. Transfection was mediated by branched polyethyleneimine (bPEI; Sigma-Aldrich), and medium was changed to fresh Opti-MEM (Life technologies) medium with 50 μg/ml gentamicin 6 h posttransfection. Virus particles were harvested 48 h after transfection by passing the supernatants through a 0.45-μm-pore filter (Sartorius) and concentrating them via ultracentrifugation in a Beckman (Beckman Coulter, Ireland) SW28 rotor at 133,000 $\times$ *g* for 1.5 h at 21°C atop a 60% (wt/vol) OptiPrep iodixanol (Sigma-Aldrich) gradient cushion. Residual OptiPrep was removed by a series of washing steps (in serum-free Opti-MEM medium), and virus particles were concentrated by ultrafiltration (Vivaspin columns, molecular weight cutoff [MWCO] 50K; Merck, Belgium).

Virus quantification. Virus production efficiency was quantified by measuring the levels of HIV-1 capsid (p24) protein by ELISA (INNOTEST p24-ELISA; Innogenetics, Ghent, Belgium) or by measuring the reverse transcriptase (RT) activity of particles present in the supernatant. p24 ELISA was performed according to the manufacturer's instructions, and RT activity was assessed by a qPCR-based SYBR green product-enhanced RT (SG-PERT) assay (50, 51).

The SG-PERT assay quantifies the cDNA reverse transcribed from an exogenous MS2 RNA template by the virus particle-associated HIV-1 RT. Viruses were lysed for 5 min (0.125% Triton X-100, 25 mM KCl, 50 mM Tris-HCl [pH 7.4], 20% [vol/vol] glycerol, 0.2 U/μl RNase inhibitor in Milli-Q [Ribolock; Thermo Fisher Scientific]) and diluted 10-fold in sample dilution buffer [5 mM $(NH_4)_2SO_4$, 20 mM KCl, 20 mM Tris-HCl (pH 8.3)]. The qPCR mix consisted of 2.5 mM $(NH_4)_2SO_4$, 10 mM KCl, 10 mM Tris-HCl (pH 8.3), 5 mM $MgCl_2$, 0.1 mg/ml bovine serum albumin (BSA), 1/5,000 SYBR green I (Thermo Fisher Scientific), 250 μM deoxynucleoside triphosphates (dNTPs), 2 μM sense primer 5′-TCCTGCTCAACTTCCTGTCGAG-3′, 2 μM antisense primer 5′-CACAGGTCAAACCTCCTAGGAATG-3′, 1 μg/ml MS2 RNA (Roche), and 0.025 U/μl TrueStart Hot Start *Taq* DNA polymerase (Thermo Fisher Scientific). Reverse transcription of the RNA template was conducted for 1 h at 37°C, followed by qPCR (to quantify the cDNA amounts), which was run on a LightCycler 480 (Roche Life Science). The qPCR program included a 5-min activation step at 95°C and 50 cycles of amplification (5 s at 95°C, 5 s at 55°C, and 15 s at 72°C).

Single-cycle virus transduction assay. One day prior to transduction, 15,000 HeLa P4 cells were seeded per well in 96-well plates and incubated in DMEM with 5% fetal bovine serum (FBS), 50 μg/ml gentamicin, and 500 μg/ml Geneticin (complete DMEM medium). The following day, the cells were transduced with equal volumes of virus supernatant in 3-fold serial dilutions, starting from the highest concentration of 100 ng p24 antigen per well. Medium was changed 24 h posttransduction to DMEM with 5% FBS, gentamicin, and Geneticin, and the cells were incubated for an additional 48 h at 37°C. Cells were washed twice with PBS and lysed by addition of lysis buffer (50 mM Tris, 200 mM NaCl, 0.2% NP-40 [vol/vol], and 5% glycerol [vol/vol]). Firefly luciferase (fLuc) activity was measured using fLuc assay reagent (ONE-Glo; Promega GMBH, Mannheim, Germany). Luciferase reporter levels were normalized for total protein content in each well by the bicinchoninic acid (BCA) assay (BCA Protein assay kit; Thermo Scientific).

Quantitative analysis of viral DNA species in transduced HeLa P4 cells. Recombinant viruses were produced as described above. HeLa P4 cells were seeded at a density of 1×10^6 cells per well in a 6-well plate and transduced 24 h later with 5 μg p24 per well of the following VSV-G pseudotyped HIV-1 particles: untagged (WT), IN-mCherry labelled (WT-mCh), dually labelled (CA-eGFP 1:2 or 1:10, depending on the ratio of CA-eGFP luciferase vector to the parental NL4-3-based construct). Transductions were carried out in the presence of DMSO or PF-03450074 (PF74; 2 μM or 10 μM). For each of the qPCR quantifications, one well of cells was left untransduced (negative control [NC]). Cells were harvested 7 days posttransduction (pt), and genomic DNA was extracted using the Sigma Mammalian genomic DNA Miniprep kit (Sigma-Aldrich) according to manufacturer's instructions. We quantified integrated viral DNA copies (integrated DNA, Gag, measured 7 days pt). qPCRs were based on Bio-Rad chemistry and

contained 1× iQ Supermix (Bio-Rad Laboratories), 300 nM forward primer, 300 nM reverse primer, 200 nM probe, and 100 ng genomic DNA. To normalize for viral DNA copy content, we used qPCR amplification of the CCR5 gene. All qPCRs and analyses were conducted as described previously (41, 52, 53). All samples were run in duplicates or triplicates. Viral DNA copies were calculated based on standard curves of highly positive samples, and signal backgrounds were estimated based on no-template controls. The qPCR was run on a LightCycler 480 (Roche Life Science), including 5-min activation at 95°C and 50 cycles of amplification (10 s at 95°C followed by 30 s at 55°C).

Transduction and immunolabelling of HeLa P4 cells for single-virus analysis. One day prior to transduction, 25,000 HeLa P4 cells were seeded per well in 8-well chamber slides (Nunc Lab-Tek chambered cover glass, 155411; Thermo Scientific), previously coated with poly-D-lysine (0.1 mg/ml; Sigma). The following day, cells were transduced with virus corresponding to 1 to 3 μg p24 antigen and fixed at designated time points. Different viral preparations were normalized for their p24 content in order to transduce the cells with comparable amounts of virus. Briefly, the cells were washed once with PBS and incubated for 45 s to 1 min at 37°C in trypsin (0.25% [wt/vol]; Life Technologies) to remove all unfused or weakly attached virus particles from the cell surface. Trypsin was inactivated by the addition of complete DMEM medium, followed by a 3-min incubation at room temperature. The cells were washed with PBS one additional time and fixed in 4% (vol/vol) paraformaldehyde (PFA) for 15 min at room temperature. After fixation, the cells were washed three times with PBS and, where indicated, stained with a lamin-specific antibody or 4′,6-diamidino-2-phenylindole (DAPI). For antibody staining purposes, the cells were permeabilized for 5 min with 0.1% (vol/vol) Triton X-100 (Sigma-Aldrich) in PBS and blocked for 30 min in blocking buffer (0.1% [vol/vol] Tween 20 [A4974; Applichem], 1% BSA [wt/vol] [Sigma-Aldrich] in PBS) at room temperature. Primary anti-lamin A/C antibody (mouse monoclonal, 1/400 dilution, sc-7292; Santa Cruz Biotechnology) was diluted in blocking buffer and incubated on cells overnight at 4°C. After extensive washing with PBS, cells were incubated in secondary anti-mouse IgG(H+L) Alexa 405 conjugate (goat polyclonal, 1/500 dilution, A-10011; Life Technologies) for 1 h at room temperature, washed, and stored in PBS at 4°C until analysis. For CA immunostaining, cells were infected with labelled viruses (see above), permeabilized, and stained with anti-lamin B1 (rabbit polyclonal, 1/400 dilution, ab16048; Abcam) and anti-CA (mouse monoclonal, 1/300 dilution, AG3.0; NIH AIDS Reagent Program, Division of AIDS, NIH [catalog number 4121] from Jonathan Allan) antibodies. The secondary antibodies used were anti-rabbit IgG(H+L) Alexa 405 conjugate (goat polyclonal, 1/500 dilution, A31556; Life Technologies) and anti-mouse IgG(H+L) Alexa 488 conjugate (goat polyclonal, 1/500 dilution, A-11001; Life Technologies).

When DAPI staining was performed, cells were not permeabilized but washed after PFA fixation and directly incubated in DAPI solution (5 μg/ml, 1/1,000 dilution in PBS; Invitrogen) for 5 min at room temperature. The cells were then washed four times in PBS and stored in PBS at 4°C until analysis.

When DMSO or HIV-1 inhibitors were used during transduction, the cells were first preincubated with DMSO or inhibitor for 2 h prior to transduction. The inhibitors used were PF74 (2 μM or 10 μM solution in DMSO, SML0835; Sigma) and RAL (0.6 μM solution in DMSO, 100× 50% inhibitory concentration [IC_{50}]; NiBSC).

Confocal microscopy and data analysis for single-virus experiments. A confocal laser scanning microscope (Fluoview FV1000; Olympus, Tokyo, Japan) was used to image the target cells and virus particles. Images were acquired using the UPLSAPO 60× water (W) numerical aperture (NA) 1.25 lens objective and a DM405/488/559/635 polychromic excitation mirror (Olympus). Fixed cells and virus particles were imaged in three-dimensional (3D) stacks, with a 0.3-μm step size and 4-μs/pixel sampling speed. To excite the fluorophores, the following lasers were used: a 488-nm laser for eGFP (emission collected at 505 to 540 nm), a 555-nm laser for mCherry (emission collected in the 575 to 675 nm range), a 405-nm laser for Alexa Fluor 405 and DAPI (emission collected at 430 to 470 nm), and a 635-nm diode laser for Alexa Fluor 633 and 647 (emission collected at 655 to 755 nm).

Fluorescent viral complexes (IN-FP and CA-eGFP) were automatically detected and localized and their intensity was measured by an in-house Matlab routine (MathWorks Inc.), as described previously (41). Since each fluorescent complex is smaller than the diffraction limit of the microscope, we calculated integrated intensity of each complex using the least mean square method after fitting the point spread function of each complex with a 2D Gaussian distribution. This was done for each z-step of the 3D image, and the highest intensity (expected to be the focus point) of each complex was used for further analysis. Viral complexes were assigned to localize to either the cytoplasm, the NE, or nucleus based on intensity thresholding of the stained nuclear lamin. The distances of fluorescent viral complexes to the nuclear lamin were calculated after the precise lamin fitting with a 2D Gaussian function, which was repeated in each z-slice (41).

In experiments where colocalization of two fluorescent complexes was assessed, the centroids were described as colocalizing in case they were found at a maximum of 2 pixels (206 nm) away from each other.

Data were collected from 30 individual cells corresponding to 500 to 1,000 viral complexes in each experiment. Experiments were repeated at least once, and the data are shown either from a representative experiment or as an average from two or three independent experiments. Data on individual complex numbers and their intensities are presented as individual data points under box-plots, with 5% and 95% whiskers. The elements of each box plot represent the following: line within the box, median value; square box, mean; bar diagrams, geometric means; error bars, back-transformed standard errors of the means. *P* values for the fluorescence intensity data were calculated by a two-sample *t* test with unequal variance of the log-normal distributed data with the following significance criteria: *P* value of <0.001 (***); *P* value of <0.01 (**), *P* value of <0.05 (*), and NS as not significant.

Mounting and immunolabelling of virus particles for microscopy. Purified virus particles were immobilized on poly-D-lysine (0.1 mg/ml)-coated 8-well chamber slides for 4 to 6 h at 37°C, washed once with PBS, and fixed with 4% PFA. After fixation, the samples were washed three times with PBS and permeabilized in 0.1% (vol/vol) Triton X-100 for 5 min at room temperature. Thereafter, the samples were washed twice in PBS and incubated in primary antibody diluted in blocking buffer (0.1% [vol/vol] Tween 20 [A4974; Applichem], 1% BSA [Sigma-Aldrich] in PBS) at 4°C overnight. The primary antibodies used were anti-HIV-1 CA (p24) (mouse monoclonal, 1/300 dilution, AG3.0; NIH AIDS Reagent Program, Division of AIDS, NIH [catalog number 4121] from Jonathan Allan), anti-HIV-1 IN (mouse monoclonal, 1/100 dilution, IN-2 ab66645; Abcam, Cambridge, UK), and anti-HIV-1 MA (p17) (rabbit polyclonal, 1/200 dilution; NIH AIDS Reagent Program, Division of AIDS, NIH [catalog number 4811] from Paul Spearman and Lingmei Ding). The secondary antibodies used were anti-mouse IgG(H+L) Alexa Fluor 405 conjugate (goat polyclonal, 1/500 dilution, A-10011; Life Technologies), anti-mouse IgG(H+L) Alexa Fluor 647 conjugate (donkey polyclonal, 1/500 dilution, A-31571; Thermo Fisher Scientific), anti-rabbit IgG(H+L) Alexa Fluor 647 conjugate (donkey polyclonal, 1/500 dilution, A-31573; Thermo Fisher Scientific), anti-mouse IgG(H+L) Alexa Fluor 647 conjugate (goat polyclonal, 1/500 to 1/500,000 dilution, 1.4 Alexa Fluor 647 molecules per antibody, 115-607-003; Dianova), and anti-mouse IgG(H+L) Alexa Fluor 633 conjugate (goat polyclonal, 1/500 dilution, A-21052; Thermo Fisher Scientific).

For particle permeabilization experiments, the viruses were mounted on poly-D-lysine coated slides as described above and subjected to mild saponin treatment as described previously (43). Saponin is a surface-acting glycoside with membrane-permeabilizing properties (54). Therefore, it punctures small pores in the viral membrane. The particles were first washed with PBS and then treated with either PBS (no saponin condition) or 100 μg/ml saponin solution in PBS (saponin condition) for 5 min at room temperature. The samples were washed once with PBS, fixed with 4% PFA, and stained as described above.

For estimating colocalization of fluorescent particle-associated proteins in purified virions, the immobilized particles were imaged in z-stacks of 6 to 12 0.3-μm steps by confocal laser scanning microscopy (CLSM). Emission from Alexa 405-stained p24, eGFP-tagged p24, and mCherry-labelled integrase (IN) was detected after excitation with lasers of 405 nm, 488 nm, and 559 nm, respectively. Confocal microscopy was conducted with a 60× apotome W NA 1.25.

Capsid core purification. Purification of intact HIV-1 cores was conducted as described previously (45). Briefly, fluorescent virus particles were produced after transient transfection of 30 10-cm dishes of 293T cells (see above). The supernatants were filtered, and virus was pelleted by ultracentrifugation (SW28 rotor, 133,000 × *g*, 2 h, 4°C) through a 20% sucrose in PBS cushion. The pelleted viruses were resuspended in a total of 1 ml of STE buffer (10 mM Tris-HCl [pH 7.4], 100 mM NaCl, 1 mM EDTA) and then subjected to core purification through layers of sucrose diluted in STE buffer. Continuous sucrose gradients (10 ml, 30% to 70% sucrose) were mounted first into ultracentrifuge tubes, covered with 0.5 ml of 15% sucrose, followed by 0.5 ml of 10% sucrose, and finally 0.5 ml virus suspension on top. The virus was split into two equal parts. One half of the virus was loaded on the control gradient (no detergent in the 15% sucrose layer), while the other virus half was loaded on a gradient with 15% sucrose layer containing 1% Triton X-100.

The particles were spun through the gradients in an SW28 rotor at 140,000 × *g* for 16 h overnight at 4°C. Afterwards, the tubes were placed on ice, and 1-ml fractions were harvested into ice-cold Eppendorf tubes. Fractions were analyzed for p24 content to determine the peak of core presence. Core-containing fractions were pooled and snap-frozen in liquid nitrogen until analysis. Before analysis, core-containing fractions were thawed on ice.

Total internal reflection fluorescence microscopy. To determine the number of fluorescent molecules incorporated into single virus particles, wide-field TIRF microscopy was performed. Quantification is possible after fluorescence intensity comparisons between purified virus particles and a single-molecule eGFP solution imaged under the same conditions. Imaging was performed on an inverted microscope (Olympus IX-83; Olympus NV, Aartselaar, Belgium) by objective-type total internal reflection excitation and wide-field detection. Excitation was performed with 488-nm (Sapphire 488-100 CW, 100 mW; Coherent) and 644-nm (Excelsior, 100 mW; Newport Spectra Physics BV) laser lines. The laser lines were combined using appropriate dichroic mirrors, and the light was circularly polarized (WPQ05M-532; Thor-labs GmbH) and expanded five times to achieve a homogenous beam profile before being focused on the back focal plane of the objective (PlanApo TIRF 60×, NA 1.45 oil; Olympus) through a 500-mm planoconvex achromatic lens (KPX211-C BK7 Precision Plano-Convex lens; Newport). Emission light was collected by the same objective and split by a polychromic mirror (z405/488/561/644rdc; Chroma) into two separate channels for eGFP detection (a HQ590/40-2P emission filter) and p24 detection (LP655). The fluorescence image was expanded 2.5-fold (PE eyepiece 125, 2.5×; Olympus) and focused onto the electron-multiplying charge-coupled device (EM-CCD) (ImagEM; Hamamatsu Photonics, Louvain-la-Neuve, Belgium). The image resolution was 512 by 512 pixels, with a pixel size of 107 nm. Movies were recorded at 100 ms per frame with continuous acquisition. Intensity was determined using Localizer software (55).

ACKNOWLEDGMENTS

We thank Paulien Van de Velde, Jooke Van der Veken, and Barbara Van Remoortel for excellent technical assistance. The following reagents were obtained through the NIH AIDS Reagent Program, Division of AIDS, NIAID, NIH: pNL4-3.Luc.R-.E- plasmid (catalog number 3418) from Nathaniel Landau, mouse monoclonal anti-HIV-1 CA (p24)

antibody (AG3.0; catalog number 4121) from Jonathan Allan, and raltegravir (catalog number 11680) from Merck and Company, Inc.

Research at KU Leuven was financially supported by the FWO, the KU Leuven Research Council (OT; OT/13/098 and C1 C14/17/095), HIV-ERA EURECA (IWT-SBO-EURECA, ZL345530), the KU Leuven IDO program (IDO/12/008), and the Belgian IAP Belvir (ZKC4893-P7/45-P).

I. Zurnic Bönisch, L. Dirix, F. Christ, J. Hendrix, J. Hofkens, and Z. Debyser conceived the study. I. Zurnic Bönisch, L. Dirix, V. Lemmens, D. Borrenberghs, and F. De Wit performed the experiments. I. Zurnic Bönisch, L. Dirix, V. Lemmens, D. Borrenberghs, F. De Wit, S. Rocha, F. Vernaillen, and Z. Debyser analyzed data. I. Zurnic Bönisch and Z. Debyser wrote the manuscript. All authors read and approved the manuscript.

We declare no conflict of interest.

REFERENCES

1. Campbell EM, Hope TJ. 2015. HIV-1 capsid: the multifaceted key player in HIV-1 infection. Nat Rev Microbiol 13:471–483. https://doi.org/10.1038/nrmicro3503.
2. Ganser BK, Li S, Klishko VY, Finch JT, Sundquist WI. 1999. Assembly and analysis of conical models for the HIV-1 core. Science 283:80–83. https://doi.org/10.1126/science.283.5398.80.
3. Li S, Hill CP, Sundquist WI, Finch JT. 2000. Image reconstructions of helical assemblies of the HIV-1 CA protein. Nature 407:409–413. https://doi.org/10.1038/35030177.
4. Briggs JAG, Simon MN, Gross I, Kräusslich H-G, Fuller SD, Vogt VM, Johnson MC. 2004. The stoichiometry of Gag protein in HIV-1. Nat Struct Mol Biol 11:672–675. https://doi.org/10.1038/nsmb785.
5. Yan N, Regalado-Magdos AD, Stiggelbout B, Lee-Kirsch MA, Lieberman J. 2010. The cytosolic exonuclease TREX1 inhibits the innate immune response to human immunodeficiency virus type 1. Nat Immunol 11:1005–1013. https://doi.org/10.1038/ni.1941.
6. Rasaiyaah J, Tan CP, Fletcher AJ, Price AJ, Blondeau C, Hilditch L, Jacques DA, Selwood DL, James LC, Noursadeghi M, Towers GJ. 2013. HIV-1 evades innate immune recognition through specific co-factor recruitment. Nature 503:402–405. https://doi.org/10.1038/nature12769.
7. Gao D, Wu J, Wu Y-T, Du F, Aroh C, Yan N, Sun L, Chen ZJ. 2013. Cyclic GMP-AMP synthase is an innate immune sensor of HIV and other retroviruses. Science 341:903–906. https://doi.org/10.1126/science.1240933.
8. Lahaye X, Satoh T, Gentili M, Cerboni S, Conrad C, Hurbain I, El Marjou A, Lacabaratz C, Lelièvre J-D, Manel N. 2013. The capsids of HIV-1 and HIV-2 determine immune detection of the viral cDNA by the innate sensor cGAS in dendritic cells. Immunity 39:1132–1142. https://doi.org/10.1016/j.immuni.2013.11.002.
9. Forshey BM, von Schwedler U, Sundquist WI, Aiken C. 2002. Formation of a human immunodeficiency virus type 1 core of optimal stability is crucial for viral replication. J Virol 76:5667–5677. https://doi.org/10.1128/jvi.76.11.5667-5677.2002.
10. Rankovic S, Varadarajan J, Ramalho R, Aiken C, Rousso I. 2017. Reverse transcription mechanically initiates HIV-1 capsid disassembly. J Virol 91:e00289-17. https://doi.org/10.1128/JVI.00289-17.
11. Mamede JI, Cianci GC, Anderson MR, Hope TJ. 2017. Early cytoplasmic uncoating is associated with infectivity of HIV-1. Proc Natl Acad Sci U S A 114:E7169–E7178. https://doi.org/10.1073/pnas.1706245114.
12. Hübner W, Chen P, Portillo AD, Liu Y, Gordon RE, Chen BK. 2007. Sequence of human immunodeficiency virus type 1 (HIV-1) Gag localization and oligomerization monitored with live confocal imaging of a replication-competent, fluorescently tagged HIV-1. J Virol 81:12596–12607. https://doi.org/10.1128/JVI.01088-07.
13. Padilla-Parra S, Marin M, Gahlaut N, Suter R, Kondo N, Melikyan GB. 2013. Fusion of mature HIV-1 particles leads to complete release of a Gag-GFP-based content marker and raises the intraviral pH. PLoS One 8:e71002. https://doi.org/10.1371/journal.pone.0071002.
14. Hulme AE, Perez O, Hope TJ. 2011. Complementary assays reveal a relationship between HIV-1 uncoating and reverse transcription. Proc Natl Acad Sci U S A 108:9975–9980. https://doi.org/10.1073/pnas.1014522108.
15. Lukic Z, Dharan A, Fricke T, Diaz-Griffero F, Campbell EM. 2014. HIV-1 uncoating is facilitated by dynein and kinesin-1. J Virol 88:13613–13625. https://doi.org/10.1128/JVI.02219-14.
16. Perez-Caballero D, Hatziioannou T, Zhang F, Cowan S, Bieniasz PD. 2005. Restriction of human immunodeficiency virus type 1 by TRIM-CypA occurs with rapid kinetics and independently of cytoplasmic bodies, ubiquitin, and proteasome activity. J Virol 79:15567–15572. https://doi.org/10.1128/JVI.79.24.15567-15572.2005.
17. Arhel NJ, Souquere-Besse S, Munier S, Souque P, Guadagnini S, Rutherford S, Prévost M-C, Allen TD, Charneau P. 2007. HIV-1 DNA Flap formation promotes uncoating of the pre-integration complex at the nuclear pore. EMBO J 26:3025–3037. https://doi.org/10.1038/sj.emboj.7601740.
18. Francis AC, Melikyan GB. 2018. Single HIV-1 imaging reveals progression of infection through CA-dependent steps of docking at the nuclear pore, uncoating, and nuclear transport. Cell Host Microbe 23:536–548. https://doi.org/10.1016/j.chom.2018.03.009.
19. Miller MD, Farnet CM, Bushman FD. 1997. Human immunodeficiency virus type 1 preintegration complexes: studies of organization and composition. J Virol 71:5382–5390.
20. Yamashita M, Emerman M. 2004. Capsid is a dominant determinant of retrovirus infectivity in nondividing cells. J Virol 78:5670–5678. https://doi.org/10.1128/JVI.78.11.5670-5678.2004.
21. Yamashita M, Perez O, Hope TJ, Emerman M. 2007. Evidence for direct involvement of the capsid protein in HIV infection of nondividing cells. PLoS Pathog 3:e156. https://doi.org/10.1371/journal.ppat.0030156.
22. Price AJ, Jacques DA, McEwan WA, Fletcher AJ, Essig S, Chin JW, Halambage UD, Aiken C, James LC. 2014. Host cofactors and pharmacologic ligands share an essential interface in HIV-1 capsid that is lost upon disassembly. PLoS Pathog 10:e1004459. https://doi.org/10.1371/journal.ppat.1004459.
23. Peng K, Muranyi W, Glass B, Laketa V, Yant SR, Tsai L, Cihlar T, Müller B, Kraüsslich H-G. 2014. Quantitative microscopy of functional HIV post-entry complexes reveals association of replication with the viral capsid. ELife 3:e04114. https://doi.org/10.7554/eLife.04114.
24. Chin CR, Perreira JM, Savidis G, Portmann JM, Aker AM, Feeley EM, Smith MC, Brass AL. 2015. Direct visualization of HIV-1 replication intermediates shows that viral capsid and CPSF6 modulate HIV-1 intra-nuclear invasion and integration. Cell Rep 13:1717–1731. https://doi.org/10.1016/j.celrep.2015.10.036.
25. Hulme AE, Kelley Z, Foley D, Hope TJ. 2015. Complementary assays reveal a low level of CA associated with viral complexes in the nuclei of HIV-1-infected cells. J Virol 89:5350–5361. https://doi.org/10.1128/JVI.00476-15.
26. Schaller T, Ocwieja KE, Rasaiyaah J, Price AJ, Brady TL, Roth SL, Hué S, Fletcher AJ, Lee K, KewalRamani VN, Noursadeghi M, Jenner RG, James LC, Bushman FD, Towers GJ. 2011. HIV-1 capsid-cyclophilin interactions determine nuclear import pathway, integration targeting and replication efficiency. PLoS Pathog 7:e1002439. https://doi.org/10.1371/journal.ppat.1002439.
27. Sowd GA, Serrao E, Wang H, Wang W, Fadel HJ, Poeschla EM, Engelman AN. 2016. A critical role for alternative polyadenylation factor CPSF6 in targeting HIV-1 integration to transcriptionally active chromatin. Proc Natl Acad Sci U S A 113:E1054–E1063. https://doi.org/10.1073/pnas.1524213113.
28. Achuthan V, Perreira JM, Sowd GA, Puray-Chavez M, McDougall WM,

Paulucci-Holthauzen A, Wu X, Fadel HJ, Poeschla EM, Multani AS, Hughes SH, Sarafianos SG, Brass AL, Engelman AN. 2018. Capsid-CPSF6 interaction licenses HIV-1 nuclear trafficking to sites of viral DNA integration. Cell Host Microbe 24:392–404. https://doi.org/10.1016/j.chom.2018.08.002.

29. Lee K, Ambrose Z, Martin TD, Oztop I, Mulky A, Julias JG, Vandegraaff N, Baumann JG, Wang J, Yuen W, Takemura T, Shelton K, Taniuchi I, Li Y, Sodroski J, Littman DR, Coffin JM, Hughes SH, Unutmaz D, Engelman A, KewalRamani VN. 2010. Flexible use of nuclear import pathways by HIV-1. Cell Host Microbe 7:221–233. https://doi.org/10.1016/j.chom.2010.02.007.
30. Rasheedi S, Shun MC, Serrao E, Sowd GA, Qian J, Hao C, Dasgupta T, Engelman AN, Skowronski J. 2016. The cleavage and polyadenylation specificity factor 6 (CPSF6) subunit of the capsid-recruited pre-messenger RNA cleavage factor I (CFIm) complex mediates HIV-1 integration into genes. J Biol Chem 291:11809–11819. https://doi.org/10.1074/jbc.M116.721647.
31. Blair WS, Pickford C, Irving SL, Brown DG, Anderson M, Bazin R, Cao J, Ciaramella G, Isaacson J, Jackson L, Hunt R, Kjerrstrom A, Nieman JA, Patick AK, Perros M, Scott AD, Whitby K, Hua W, Butler SL. 2010. HIV capsid is a tractable target for small molecule therapeutic intervention. PLoS Pathog 6:e1001220. https://doi.org/10.1371/journal.ppat.1001220.
32. Shi J, Zhou J, Shah VB, Aiken C, Whitby K. 2011. Small-molecule inhibition of human immunodeficiency virus type 1 infection by virus capsid destabilization. J Virol 85:542–549. https://doi.org/10.1128/JVI.01406-10.
33. Fricke T, Brandariz-Nuñez A, Wang X, Smith AB, Diaz-Griffero F. 2013. Human cytosolic extracts stabilize the HIV-1 core. J Virol 87:10587–10597. https://doi.org/10.1128/JVI.01705-13.
34. Fricke T, Buffone C, Opp S, Valle-Casuso J, Diaz-Griffero F. 2014. BI-2 destabilizes HIV-1 cores during infection and prevents binding of CPSF6 to the HIV-1 capsid. Retrovirology 11:120. https://doi.org/10.1186/s12977-014-0120-x.
35. Zhou J, Price AJ, Halambage UD, James LC, Aiken C. 2015. HIV-1 resistance to the capsid-targeting inhibitor PF74 results in altered dependence on host factors required for virus nuclear entry. J Virol 89:9068–9079. https://doi.org/10.1128/JVI.00340-15.
36. Campbell EM, Perez O, Anderson JL, Hope TJ. 2008. Visualization of a proteasome-independent intermediate during restriction of HIV-1 by rhesus TRIM5α. J Cell Biol 180:549–561. https://doi.org/10.1083/jcb.200706154.
37. Pereira CF, Ellenberg PC, Jones KL, Fernandez TL, Smyth RP, Hawkes DJ, Hijnen M, Vivet-Boudou V, Marquet R, Johnson I, Mak J. 2011. Labelling of multiple HIV-1 proteins with the biarsenical tetracysteine system. PLoS One 6:e17016. https://doi.org/10.1371/journal.pone.0017016.
38. Martin BR, Giepmans BNG, Adams SR, Tsien RY. 2005. Mammalian cell-based optimization of the biarsenical-binding tetracysteine motif for improved fluorescence and affinity. Nat Biotechnol 23:1308–1314. https://doi.org/10.1038/nbt1136.
39. Chen B-C, Legant WR, Wang K, Shao L, Milkie DE, Davidson MW, Janetopoulos C, Wu XS, Hammer JA, Liu Z, English BP, Mimori-Kiyosue Y, Romero DP, Ritter AT, Lippincott-Schwartz J, Fritz-Laylin L, Mullins RD, Mitchell DM, Bembenek JN, Reymann AC, Böhme R, Grill SW, Wang JT, Seydoux G, Tulu US, Kiehart DP, Betzig E. 2014. Lattice light-sheet microscopy: imaging molecules to embryos at high spatiotemporal resolution. Science 346:1257998. https://doi.org/10.1126/science.1257998.
40. Albanese A, Arosio D, Terreni M, Cereseto A. 2008. HIV-1 pre-integration complexes selectively target decondensed chromatin in the nuclear periphery. PLoS One 3:e2413. https://doi.org/10.1371/journal.pone.0002413.
41. Borrenberghs D, Dirix L, De Wit F, Rocha S, Blokken J, De Houwer S, Gijsbers R, Christ F, Hofkens J, Hendrix J, Debyser Z. 2016. Dynamic oligomerization of integrase orchestrates HIV nuclear entry. Sci Rep 6:36485. https://doi.org/10.1038/srep36485.
42. Borrenberghs D, Thys W, Rocha S, Demeulemeester J, Weydert C, Dedecker P, Hofkens J, Debyser Z, Hendrix J. 2014. HIV virions as nanoscopic test tubes for probing oligomerization of the integrase enzyme. ACS Nano 8:3531–3545. https://doi.org/10.1021/nn406615v.
43. Francis AC, Marin M, Shi J, Aiken C, Melikyan GB. 2016. Time resolved imaging of single HIV1 uncoating *in vitro* and in living cells. PLoS Pathog 12:e1005709. https://doi.org/10.1371/journal.ppat.1005709.
44. Márquez CL, Lau D, Walsh J, Shah V, McGuinness C, Wong A, Aggarwal A, Parker MW, Jacques DA, Turville S, Böcking T. 2018. Kinetics of HIV-1 capsid uncoating revealed by single-molecule analysis. Elife 7:e34772. https://doi.org/10.7554/eLife.34772.
45. Shah VB, Aiken C. 2011. *In vitro* uncoating of HIV-1 cores. J Vis Exp 2011:3384. https://doi.org/10.3791/3384.
46. Ambrose Z, Aiken C. 2014. HIV-1 uncoating: connection to nuclear entry and regulation by host proteins. Virology 454–455:371–379. https://doi.org/10.1016/j.virol.2014.02.004.
47. Matreyek KA, Yücel SS, Li X, Engelman A. 2013. Nucleoporin NUP153 phenylalanine-glycine motifs engage a common binding pocket within the HIV-1 capsid protein to mediate lentiviral infectivity. PLoS Pathog 9:e1003693. https://doi.org/10.1371/journal.ppat.1003693.
48. He J, Choe S, Walker R, Di Marzio P, Morgan DO, Landau NR. 1995. Human immunodeficiency virus type 1 viral protein R (Vpr) arrests cells in the G_2 phase of the cell cycle by inhibiting p34cdc2 activity. J Virol 69:6705–6711.
49. Chiu J, March PE, Lee R, Tillett D. 2004. Site-directed, Ligase-Independent Mutagenesis (SLIM): a single-tube methodology approaching 100% efficiency in 4 h. Nucleic Acids Res 32:e174. https://doi.org/10.1093/nar/gnh172.
50. Pizzato M, Erlwein O, Bonsall D, Kaye S, Muir D, McClure MO. 2009. A one-step SYBR green I-based product-enhanced reverse transcriptase assay for the quantitation of retroviruses in cell culture supernatants. J Virol Methods 156:1–7. https://doi.org/10.1016/j.jviromet.2008.10.012.
51. Vermeire J, Naessens E, Vanderstraeten H, Landi A, Iannucci V, Van Nuffel A, Taghon T, Pizzato M, Verhasselt B. 2012. Quantification of reverse transcriptase activity by real-time PCR as a fast and accurate method for titration of HIV, lenti- and retroviral vectors. PLoS One 7:e50859. https://doi.org/10.1371/journal.pone.0050859.
52. Vansant G, Vranckx LS, Zurnic I, Van Looveren D, Van de Velde P, Nobles C, Gijsbers R, Christ F, Debyser Z. 2019. Impact of LEDGIN treatment during virus production on residual HIV-1 transcription. Retrovirology 16:8. https://doi.org/10.1186/s12977-019-0472-3.
53. Thys W, De Houwer S, Demeulemeester J, Taltynov O, Vancraenenbroeck R, Gérard M, De Rijck J, Gijsbers R, Christ F, Debyser Z. 2011. Interplay between HIV entry and transportin-SR2 dependency. Retrovirology 8:7. https://doi.org/10.1186/1742-4690-8-7.
54. Francis G, Kerem Z, Makkar HP, Becker K. 2002. The biological action of saponins in animal systems: a review. Br J Nutr 88:587–605.
55. Dedecker P, Duwe S, Neely RK, Zhang J. 2012. Localizer: fast, accurate, open-source, and modular software package for superresolution microscopy. J Biomed Opt 17:126008. https://doi.org/10.1117/1.JBO.17.12.126008.
56. Reference deleted.
57. Bhattacharya A, Alam SL, Fricke T, Zadrozny K, Sedzicki J, Taylor AB, Demeler B, Pornillos O, Ganser-Pornillos BK, Diaz-Griffero F, Ivanov DN, Yeager M. 2014. Structural basis of HIV-1 capsid recognition by PF74 and CPSF6. Proc Natl Acad Sci U S A 111:18625–18630. https://doi.org/10.1073/pnas.1419945112.
58. Briggs JAG, Wilk T, Welker R, Kräusslich H-G, Fuller SD. 2003. Structural organization of authentic, mature HIV-1 virions and cores. EMBO J 22:1707–1715. https://doi.org/10.1093/emboj/cdg143.
59. McDonald D, Vodicka MA, Lucero G, Svitkina TM, Borisy GG, Emerman M, Hope TJ. 2002. Visualization of the intracellular behavior of HIV in living cells. J Cell Biol 159:441–452. https://doi.org/10.1083/jcb.200203150.
60. Borrenberghs D, Zurnic I, De Wit F, Acke A, Dirix L, Cereseto A, Debyser Z, Hendrix J. 2019. Post-mitotic BET-induced reshaping of integrase quaternary structure supports wild-type MLV integration. Nucleic Acids Res 47:1195–1210. https://doi.org/10.1093/nar/gky1157.
61. Stirnnagel K, Lüftenegger D, Stange A, Swiersy A, Müllers E, Reh J, Stanke N, Grosse A, Chiantia S, Keller H, Schwille P, Hanenberg H, Zentgraf H, Lindemann D. 2010. Analysis of prototype foamy virus particle-host cell interaction with autofluorescent retroviral particles. Retrovirology 7:45. https://doi.org/10.1186/1742-4690-7-45.
62. Verkhusha VV, Sorkin A. 2005. Conversion of the monomeric red fluorescent protein into a photoactivatable probe. Chem Biol 12:279–285. https://doi.org/10.1016/j.chembiol.2005.01.005.